Dynamics in Turbulence

Thesis

The Open University

MPhil in Applied Mathematics

Dynamics in Turbulence

Harry Robert Kennard BA (Oxon) MAST (Cantab)

8th August 2013

Date of Submission: 8 August 2013
Date of Award: 2 December 2013

ProQuest LLC.
789 East Eisenhower Parkway
P.O. Box 1346
Ann Arbor, MI 48106 – 1346

Abstract

This MPhil thesis explores two themes associated with the dynamics of inertial particles in turbulent fluids. Firstly, we consider an optimal partial covering of fractal sets in a two-dimensional space using ellipses which become increasingly anisotropic as their size is reduced. If the semi-minor axis is ϵ and the semi-major axis is δ, we set $\delta = \epsilon^{\alpha}$, where $0 < \alpha < 1$ is an exponent characterizing the anisotropy of the ellipses. The optimization involves varying the angle of the principal axis to maximize the measure covered by each ellipse. For point set fractals, in most cases we find that the number of points $\mathcal{N}$ which can be covered by an ellipse centred on any given point has expectation value $\langle \mathcal{N} \rangle \sim \epsilon^{\beta}$, where β is a generalized of the fractal dimension . $\beta(\alpha)$ is investigated numerically for various sets, showing that it may be different for sets which have the same fractal dimension.
Secondly, we examine an analytically solvable limit of a model for the alignment of microscopic rods in a random velocity field with isotropic statistics. The vorticity varies very slowly and the isotropic random flow is equivalent to a pure strain with statistics which are axisymmetric about the direction of the vorticity. We analyse the alignment in a weakly fluctuating uniaxial strain field, as a function of the product of the strain relaxation time τ_s and the angular velocity ω about the vorticity axis. We find that when $\tau_s \omega >> 1$, the rods are predominantly either perpendicular or parallel to the vorticity. We also review the current literature on the dynamics of inertial particles in turbulent flows.

Contents

Chapter 1

Introduction and Background

The central focus of this MPhil is to explore and contribute to current understanding of inertial particles in turbulent flows.

> Shall I say, I have gone at dusk through narrow streets
> And watched the smoke that rises from the pipes
> Of lonely men in shirt-sleeves, leaning out of windows?...
>
> *T. S. Eliot* [1]

1.1 Motivation

The problem of understanding the behaviour of particles suspended in fluid flows is not new. Since ancient times, humans have surely pondered the swirls, whorls and arabesques that are formed as smoke rises from fire; or the dynamics of billowing clouds as they drift across the sky. Indeed, there are manifold other physical instances in which microscopic particles are carried along by a moving fluid (advection), (figure 1.1 shows yet another example). In more recent times, the time scale of rain initiation is cited as being a prominent example of a problem that pertains to particles suspended in turbulent flows (see for example [2, 3, 4]). However, many other applications exist, from modelling blood flow [5] to planet formation [6] as well as countless industrial and manufacturing processes. This thesis, however, concerns only the mathematical properties of such flows. In particular we focus on two distinct questions: what are the isotropy properties of the distributions that particles take when suspended in quasi-turbulent flows, and how does particle geometry affect the mean orientation of particles in such flows. The work undertaken for this thesis has been published in two papers, both in the Journal of Physics A [7, 8]. All work was conducted under the supervision of Professor Michael Wilkinson of the Open University, while the write up stage was supervised by Professor Uwe Grimm of the Open University. Professor Michael Morgan of Seattle University was a collaborator for the

Figure 1.1: This photograph shows the structure of minute bubbles on the surface of the sea shortly after a wave has broken.

work [7] which forms chapter 3.

The structure of the thesis is as follows: Chapter 1 concerns introductory themes, and motivates the work conducted. Chapter 2 consists of a survey of the current field. Chapters 3 and 4 contain the content of the published papers. We give a brief outline of the themes of these papers before proceeding to a more general introduction to the field.

Chapter 3 concerns the development of a new measure of anisotropy, the utility of which will be expounded. We consider an optimal partial covering of fractal sets in a two-dimensional space using ellipses which become increasingly anisotropic as their size is reduced. If the semi-minor axis is ϵ and the semi-major axis is δ, we set $\delta = \epsilon^{\alpha}$, where $0 < \alpha < 1$ is an exponent characterizing the anisotropy of the ellipses. The optimization involves varying the angle of the principal axis to maximize the measure covered by each ellipse. For point set fractals, in most cases we find that the number of points $\mathcal{N}$ which can be covered by an ellipse centred on any given point has expectation value $\langle \mathcal{N} \rangle \sim \epsilon^{\beta}$, where β is a generalization of the fractal dimension (see 1.3.1). We coin the portmanteau *spectal* dimension for the function β, because of links to specular light scattering from fractal sets. $\beta(\alpha)$ is investigated numerically for various sets, showing that it may be different for sets which have the same fractal dimension.

Chapter 4 examines an analytically solvable limit of a model for the alignment of microscopic rods in a random velocity field with isotropic statistics. The vorticity varies very slowly and the isotropic random flow is equivalent to a pure strain with statistics which are axisymmetric about the direction

of the vorticity. We analyse the alignment in a weakly fluctuating uniaxial strain field, as a function of the product of the strain relaxation time τ_s and the angular velocity ω about the vorticity axis. We find that when $\tau_s\omega >> 1$, the rods are predominantly either perpendicular or parallel to the vorticity. Finally, closing remarks are made in chapter 5.

1.2 Preliminaries

Inertial particles have non-zero mass and are transported when suspended in a moving fluid flow along paths which, in general, differ from particles of zero mass (tracers). Fluid flow is described by the Navier-Stokes equations (NS) which in the absence of external forces such as gravity is

$$\frac{\partial \boldsymbol{u}}{\partial t} + \boldsymbol{u} \cdot \nabla \boldsymbol{u} = -\frac{\nabla \boldsymbol{p}}{\rho} + \nu \nabla^2 \boldsymbol{u} \tag{1.1}$$

where $\boldsymbol{u}$ is the fluid flow velocity, $\boldsymbol{p}$ the pressure, ν the kinematic viscosity and ρ the density. Incompressibility of the flow adds the further condition that $\nabla \cdot \boldsymbol{u} = 0$. Turbulent flow is characterised by the dimensionless Reynolds number Re. Typically, high Re flows result in chaotic and irregular motion of the fluid. Turbulent flow is contrasted with laminar flow (typically small Re) in which flow is regular and smooth. Re is defined

$$Re = \frac{vL}{\nu} \tag{1.2}$$

where v is the mean fluid velocity, L the typical length scale of the system and ν the kinematic viscosity. This relationship means that fast flowing fluids will typically have high Reynolds number and hence tend to be turbulent (although certain features can prevent this from being the case). The Reynolds number of a golf ball moving at around 35 m/s is approximately 1×10^5, and the flow is turbulent. However, there is no complete theorem which tells us whether a flow of a given Re will be turbulent or not, indeed a complete understanding of turbulent flows remains one of the last unsolved of classical physics. Despite this, substantial progress has been made, perhaps most notably through the work of Andrey Kolmogorov in the middle part of the 20th century.

1.2.1 Kolmogorov 1941

One of the most important aspects of turbulent flow is the 'cascade', neatly summed up by Richardson in his poem,

> *'Big whirls have little whirls that feed on their velocity, and little whirls have lesser whirls, and so on to viscosity.'* Richardson, (1922)

Cascades arise when energy is transferred from one scale to another due to a difference between the scale at which energy enters a systems and the scale at which dissipation occurs. A car moving at high speed through air has a typical length scale of around a couple of meters and yet viscous friction (the

dissipative scale) is found at lengths of millimetres. The interval between the input and output energy is known as the inertial interval. Cascades need not always happen in this manner. Accreting matter in space clumps together under gravity and the size of the average clump of matter increases with time. In this case the process is termed an 'inverse cascade' because the process involves flux from small to large scales. Inverse cascades also occur in two dimensional turbulence but such processes shall not be considered further here, for more information see [9].

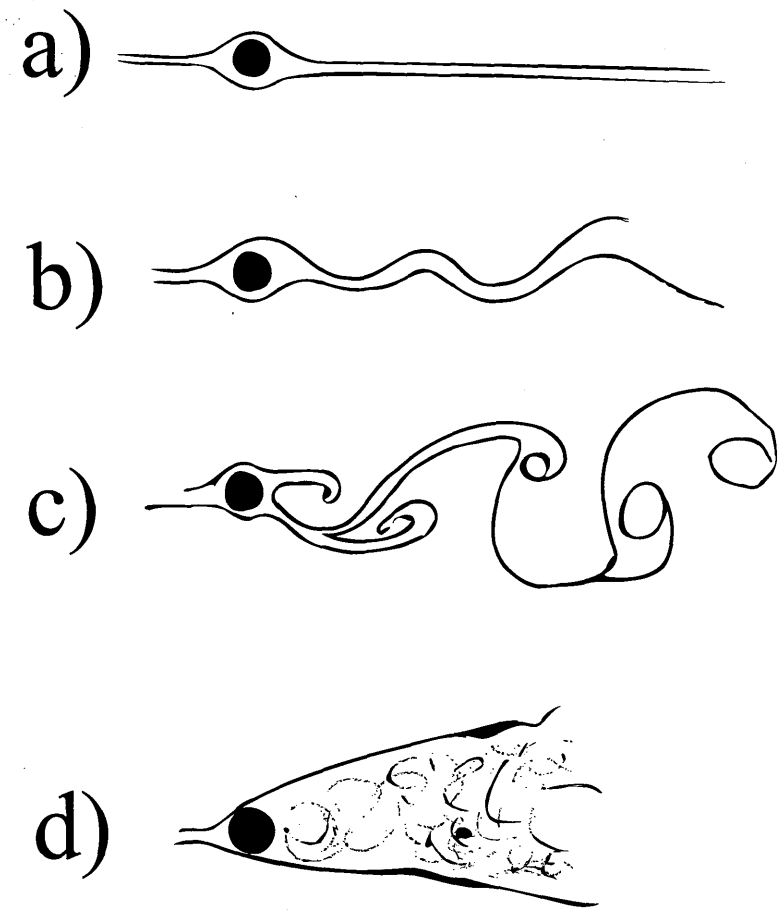

Figure 1.2: A schematic diagram of flow past a cylinder (viewed from above). Stream lines are visualised for increasing Reynolds number. a) shows smooth laminar at low Reynolds number. b) As the Reynolds number increases the symmetry of the flow is broken and instabilities manifest themselves as periodic structure c) the so Von Karman vortex street is established in which the periodic structure develops into vortices. d) the Reynolds number is so high that the flow becomes statistically isotropic (within the plume) in line with Kolmogorov's theory.

In 1941 Kolmogorov (K41) postulated that for fully developed turbulence (the limit of very high Reynolds number) the turbulence is statistically isotropic. An additional assumption to K41 theory is that of *universality*, that sufficiently far from boundaries all turbulent flows are statistically the same, and independent of the means by which the turbulence was generated. This is equivalent to the statement that any symmetries of the flow that are broken at intermediate Re (see figure 1.2) will be restored, in a statistical sense, at the limit of very large Re. Experiment has largely supported this hypothesis [10].

1.2.2 Computational Fluid Dynamics

Simulating turbulence using computers is a highly complex task. Broadly there are two approaches one can adopt. Firstly, direct numerical simulation (DNS) seeks to directly solve the NS equations by means of a discretisation of space-time. The second approach, called *synthetic* turbulence exploits the statistical properties of turbulence and generates a random field which seeks to mimic the physically significant aspects of turbulent flows.

DNS

DNS methods are numerous and well developed. The general scheme involves [11] simplifying the differential operators of the NS equations by a discrete approximation to it. The following table (adapted from [11]) briefly outlines the various approaches that may be adopted. Generally speaking DNS requires a large amount of computing time compared to synthetic turbulence methods.

Method	Abbreviation	Description
Finite-Difference Methods	FDM	Replace differential operators by combinations of translation operators that can be derived from Taylor series.
Finite-Volume Methods	FVM	Integral formulations replace Taylor series (which may not converge). Flux between discrete cells key.
Finite-Element Method	FEM	Approximates PDE (of NS equations) with a system of ordinary differential equations
Spectral Methods	SM	Uses truncated series of orthogonal basis functions. Fourier, Chebyshev or Legendre series common. High accuracy

Synthetic Turbulence

Synthetic turbulence simulations differ from DNS in the sense that they do no seek to reproduce all of the flow structure directly, but rather use statistical methods to produce the most important aspects of a flow (self similarity for example, as well as the form of probability density functions associated with the flow) Much work has been conducted on producing *synthetic* flows that capture the appropriate aspects of the flow (for an overview see [12]). Flows are created by generating random fields with statistics that match, in as many aspects as possible, those of turbulent flows.

1.2.3 Clustering

The problem of understanding how inertial particles suspended in turbulent flows behave has received much attention and is of great importance to many physical systems. The distribution of tracer particles in turbulence is homogeneous, they will move ergodically following the flow and sample all positions within the flow with equal likelihood. However, when inertia is introduced into the particles their path will change, and inhomogeneity can arise. In order to understand this result, the relevant equations of motion are considered. Maxey and Riley [13] give us the following equation of motion for a particle moving in a fluid. The effect of fluid displaced by the particle is neglected for simplicity. $\boldsymbol{r}$ is the position of a particle and γ is the rate at which the particles relax towards the fluid velocity, and where $\boldsymbol{u}(\boldsymbol{r},t)$ is a randomly fluctuating velocity field satisfying the incompressibility condition $\boldsymbol{\nabla}\cdot\boldsymbol{u}=0$

$$\dot{\boldsymbol{r}}=\boldsymbol{v}\ , \quad \dot{\boldsymbol{v}}=-\gamma[\boldsymbol{v}-\boldsymbol{u}(\boldsymbol{r}(t),t)] \tag{1.3}$$

Particles in the fluid flow cluster if the damping time-scale γ^{-1} is comparable to a time-scale characterising the velocity field. The importance of inertial effects can be characterised by a dimensionless parameter η, this characterisation will be used in the discussions below. It is defined in terms of the correlation function of the velocity gradient experienced by a particle with trajectory $\boldsymbol{r}(t)$:

$$\eta^2(\gamma)=\frac{1}{2\gamma}\int_{-\infty}^{\infty}\mathrm{d}t\ \left\langle\left(\frac{\partial u_x}{\partial x}\right)(\boldsymbol{r}(t),t)\left(\frac{\partial u_x}{\partial x}\right)(\boldsymbol{0},0)\right\rangle\ . \tag{1.4}$$

Two physical process have been identified which lead to inhomogeneity and clustering in the particle's distribution. These process are known as preferential concentration and the sling effect (which is due to caustic formation; see section 2.3).

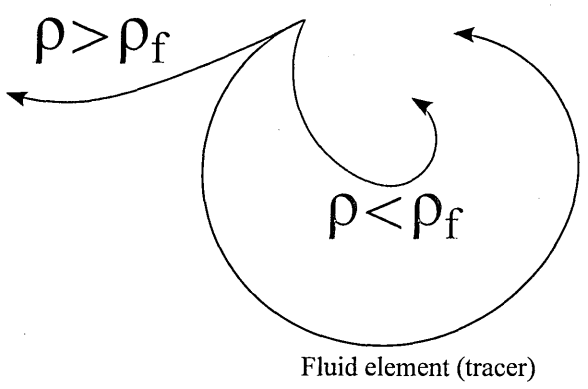

Figure 1.3: Particles with greater density ρ than the fluid are advected out of vortices (the sling effect) and those with a lower density concentrated within vortices (preferential concentration)

Clustering in random flows was first described in one dimension by Deutsch [14]. Around a similar time Maxey and Riley [13] identified 'preferential concentration' as a mechanism by which light particles are concentrated within regions of high vorticity and heavy particles in regions of high

strain. However, certain flows exhibit clustering where preferential concentration is absent, notably Kraichnan flows [15]. As Olla points out, 'the concepts of strain and vorticity do not exist in one dimension. This casts some doubts on whether preferential concentration (or some generalized version of it) is an essential ingredient for inertial particle clustering in random flows' [16]. As such no complete picture has been arrived at which describes all relevant mechanisms of particle clustering, despite a great deal of progress having been made. The current state of the literature on particles in turbulent flows will be outlined in chapter 2.

1.3 Key concepts

In this section we expound key concepts that shall be used in this thesis. The explanations given here are not intended to be exhaustive explanations, rather summaries intended to aid the comprehension of the following chapters.

1.3.1 Fractal

The word 'fractal' was first coined by Mandelbrot in the 1970's and is used to describe any structure which exhibits self similarity across a large number of distance scales. Formally a fractal has continuous scaling symmetry, but in physical systems such scaling cannot extend *all the way down* (figure 1.4 shows a fractal with five generations). Any structure which exhibits self similarity tends to be called a fractal if self similarity extends over a few generations, and typically suggests that the underlying equations have an attractor (the limiting form) which would be a true fractal were it not for size limitations imposed by something that breaks the scaling symmetry such as cellular structure in plants, or molecular structure in snowflakes.

Cantor Set

The archetypal fractal is perhaps the Cantor set. It was first described by Gregor Cantor in 1883 [17], long before Mandelbrot coined the generic term for self similar objects. The construction of the Cantor set is straightforward and very well known, but it shall be referred to in this thesis so it is worth covering. Consider the unit interval, remove the open central third and two intervals remain, spanning $[0, \frac{1}{3}]$ and $[\frac{2}{3}, 1]$. The same process is then repeated to these intervals and the central thirds of the remaining intervals removed. As this process is repeated more of the initial interval is removed, but some points remain. The remaining points are a fractal set of zero measure (which is considered in this thesis to be synonymous with mass) yet an infinite number of points. The first few steps of this process are illustrated in figure 1.4.

The fractal dimension of a set is a key concept which is employed in this thesis. The fractal dimension [18, 19] is a quantity that is ascribed to sets that are deemed to be fractal to capture their dimensional character, in the same manner that euclidean dimensions differentiates between planar

Figure 1.4: The first few iterations involved in the construction of the Cantor set. The object has a limiting dimension of $D = \frac{\log 2}{\log 3}$.

and solid figures by using integer number spatial dimensions. It is often (though not necessarily) the case that the fractal dimension of a fractal set will lie between whole numbers. There are multiple methods for determining the fractal dimension of a set, but for the purpose of clarity we start with the box counting dimension.

Box counting

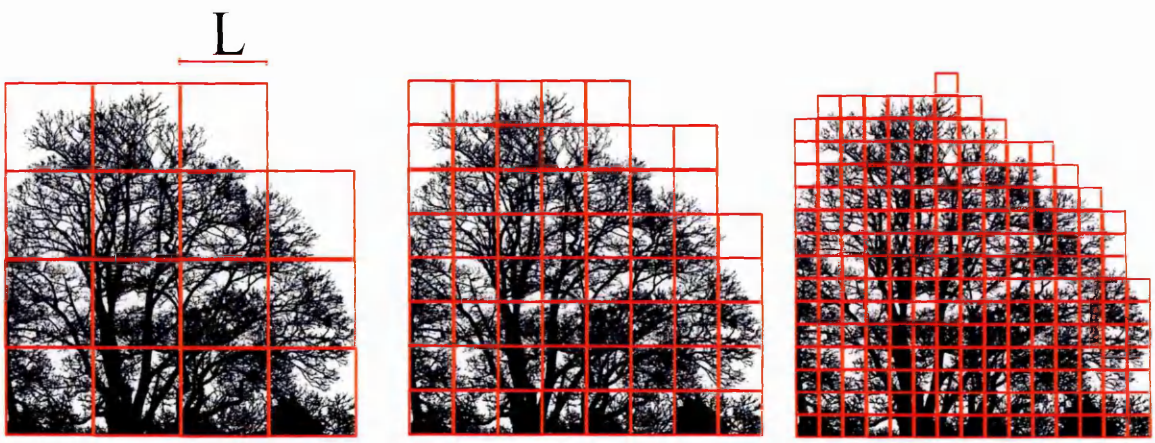

Figure 1.5: Box counting for a photograph of a tree. Here $D_0 \approx 1.8$

The box counting dimension is perhaps the simplest of all the fractal dimensions to visualise. It is computed by the following method: First, cover the set in boxes of size L, noting how many boxes N contain some element of the set 1.5. Reduce L and repeat the process. The resultant box counting dimension is therefore defined thus, so long as the limit exists

$$D_0 = \lim_{L \to 0} \frac{\log N}{\log(1/L)} \tag{1.5}$$

When applied to the simple Cantor set it is easy to see that the box counting dimension must be $\frac{\log 2}{\log 3}$ since it contains 2 copies of itself, each a third the size of the original object.

Multifractal

A multifractal (see [19] for examples) is any fractal which has more than one scaling length associated with it. Multifractals contrast the simple fractal (such as the Cantor set) discussed above as the density of points will vary from place to place within them giving them the appearance of a greyscale image. They can result from dynamic maps such as the Hénon map (see [20] for details of the fractal dimension of this set) as well as the inertial particles in random flow model discussed in this thesis. The Renyi dimension D_q is a multicomponent dimension, using a subscript q which is sensitive to the multi-scaling nature of multifractals and is defined as

$$D_q = \lim_{L \to 0} \frac{\frac{1}{1-q} \log \sum_i {p_i}^q}{\log(1/L)} \tag{1.6}$$

where $q \neq 1$ and p gives the probability of finding a member of the set in a particular box. High density regions of the fractal are therefore weighted by the subscript q. For $q = 0$, D_q is simply the box counting dimension. For simple *mono-fractals* with only scaling length associated with them all D_q have the same value. However, for a multifractal D_q will be a monotonically decreasing function of q. The $q = 1$ case is known as the information dimension and will not be used in this thesis. In this thesis we pay particular attention to the case where $q = 2$. This particular value is referred to as the *correlation dimension* and has multiple connections to other aspects of dynamical systems theory. It can be calculated using the Renyi form, or using an equivalent definition (see [21] for details of derivation)

$$D_2 = \lim_{L \to 0} \frac{\log C(L)}{\log L} \tag{1.7}$$

where $C(L)$ is the correlation integral, which is defined by

$$C(L) = \lim_{N \to \infty} \frac{g}{N^2} \tag{1.8}$$

and g is number of pairs that are less than some distance L away from each other. For large L $C(L) \approx L^{D_2}$. It is attributed the name *correlation* dimension because it captures the degree of correlation between adjacent points in the set.

1.3.2 Stochastic Physics

A key component of this thesis shall be the use of stochastic physics for the modelling of random flows. Here we review and introduce some concepts which will be essential for understanding the following chapters.

Random Walk

The random walk is perhaps the simplest stochastic process. The 1-dimensional random walk consists of a particle which starts at the origin. At each step of the process the walker either goes left or right (with equal probability) a distance of one unit. The probability that the walker will end up a distance d away from the origin after N steps in the limit of large N is given by

$$P_N(d) = \frac{1}{2^N}\binom{N}{\frac{d+N}{2}} \tag{1.9}$$

as is shown in [22]. Grünbaum [23] gives the expected distance travelled as

$$\langle d_n \rangle \approx \sqrt{\frac{2N}{\pi}} \tag{1.10}$$

which means that a random walker will escape to infinity, even if it has an equal chance going left or right. The continuous time and space limit of the random walk is known as a Wiener process. The correspondence between the random walk and Wiener process is analogous to the relationship between the binomial and normal distribution. The Wiener process provides a good model for random Brownian motion [24]

Langevin Equation

The Langevin equation for the motion of particle undergoing Brownian motion is

$$\dot{v} = -\gamma\dot{x} + \xi(t) \tag{1.11}$$

where γ is the drag force per unit mass and $\xi(t)$ a random force with $\langle \xi(t) \rangle = 0$ and $\langle \xi(t)\xi(t') \rangle = 2D\delta(t - t')$ where D is a diffusion constant.

Ornstein Uhlenbeck Process

An Ornstein Uhlenbeck (OU) process acts in a similar manner as the Langevin equation, but has a damping term which forces motion back toward the mean. In contrast to the Wiener process which models the position of the Brownian particle the OU process can used to model the stochastic behaviour of the *velocity* of the Brownian particle. In this sense the OU process is applicable to so-called mean reverting behaviour, which is evident through the presence of the drift term.

$$\dot{x} = -\gamma x + \eta(t) \tag{1.12}$$

where $\langle \eta(t) \rangle = 0$ and $\langle \eta(t)\eta(t') \rangle = 2D\delta(t - t')$

Fokker-Planck equation

The Langevin equation is a special case of the more general equation

$$\frac{dz}{dt} = a(z,t) + b(z,t)\Gamma(t) \tag{1.13}$$

where $a(z,t)$ and $b(z,t)$ simply govern the relative importance of deterministic and stochastic terms and the stochastic force has the usual statistics $\langle\Gamma(t)\rangle = 0$ and $\langle\Gamma(t)\Gamma(t')\rangle = \delta(t-t')$. Typically they can be determined from knowledge of the average behaviour of a physical system (see for example [25]). The equation that governs the evolution of probability density of a particular process governed by the OU process is the Fokker-Plank equation. This equation can be thought of as a generalisation of the diffusion equation with the addition of drift.

$$\frac{\partial P(x,t)}{\partial t} = -\frac{\partial aP(x,t)}{\partial x} + \frac{1}{2}\frac{\partial^2 b^2 P(x,t)}{\partial^2 t} \tag{1.14}$$

For a full derivation of (1.14) see [25].

1.3.3 Other Concepts

Baker map

It is worthwhile including a reference to a simple dynamical map. There are numerous complex maps in dynamical systems theory [26], but the Baker's map provides an insightful example of the behaviour which is typical to many maps. The map is defined in the following manner

$$B(x,y) = \begin{cases} (2x, y/2) & \text{for } 0 \leq x < 1/2 \\ (2x-1, 1/2+y/2), & \text{for } 1/2 \leq x < 1 \end{cases} \tag{1.15}$$

and geometrically realised in figure 1.6 applied to a photograph. The reason why this particular map is called the Baker's Map is evident, since the stretching and cutting of a kneading baker is evident. It demonstrates the mixing that occurs under the action of a dynamical map. The action of inertial particles in a random flow can be thought of as complex map, which mixes phase space in an analogous (but not reversible) manner.

Lyapunov Exponents

A Lyapunov exponent is a measure of the rate at which infinitesimally close regions of phase space diverge. For a one dimensional system, given an initial separation of δX_0 the Lyapunov exponent λ is given by

$$|X(t)| \approx e^{\lambda t}|\delta X_0| \tag{1.16}$$

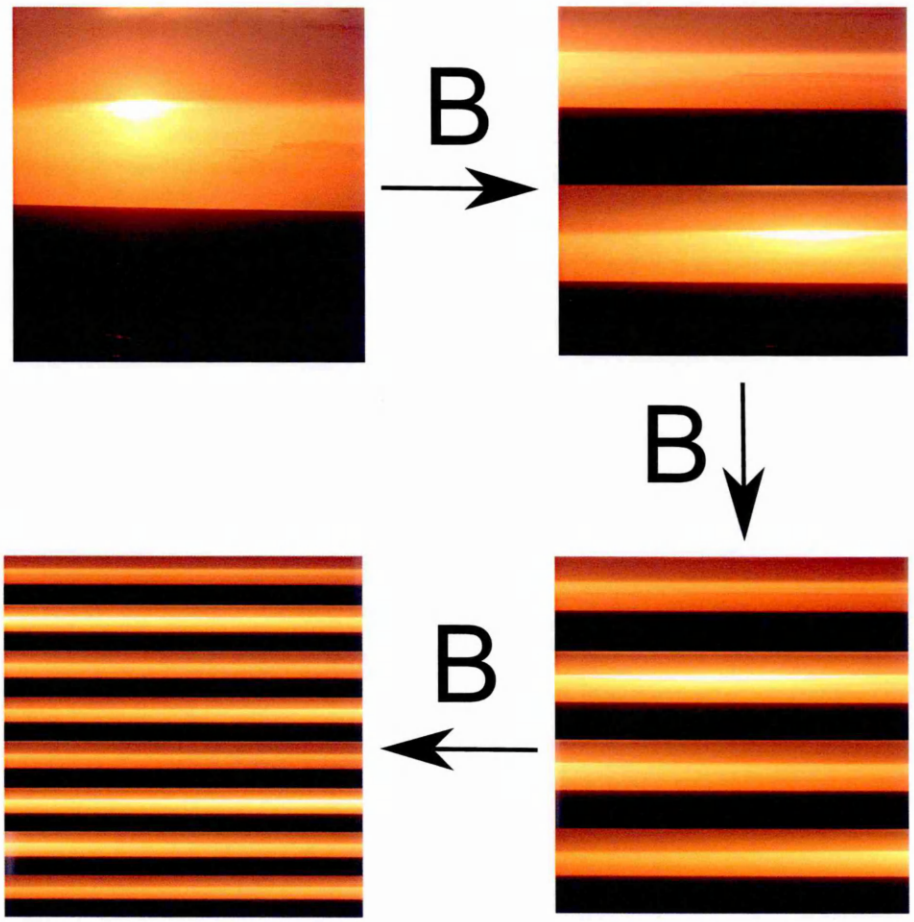

Figure 1.6: Baker's map B applied three times to a photograph of the sunset. Mixing of the phase space is evident. (Photo credit: Ahmad N. Hejazy with permission)

For phases spaces of dimension 2 or greater the scalar λ becomes a vector $\boldsymbol{\lambda}$, the largest component of which is termed the 'Maximal Lyapunov exponent' (MLE). The Cartesian product is a straightforward multiplication process applied to two sets X and Y which produces all ordered pairs (x, y) where x and y are the members of sets X and Y respectively. For the sets we will consider, that is to say ones that are reasonably behaved, the dimension of sets produced by the Cartesian product is equal to the sum of the dimensions of the sets X and Y (for examples of sets which do not behave well, see [19] p.99). The fact that pairs are ordered means the product is necessarily non-commutative. The resultant set is two dimensional and is easier to visual in the example given in figure 1.7. The definition of the Cartesian product suggests that certain two dimensional sets may be decomposed as the Cartesian of two lower dimensional sets this shall prove useful in section 3

1.3.4 Methods

We give a brief note of the methods used to produce the data in this thesis. Numerical work was done using FORTRAN and simulations run either locally or the Open University's Cluster (IMPACT). More detailed descriptions of specific algorithms used is given in the appropriate sections. Analytic work that required it was using MAPLE 6. Figures were created using both GNUPLOT and Inkscape.

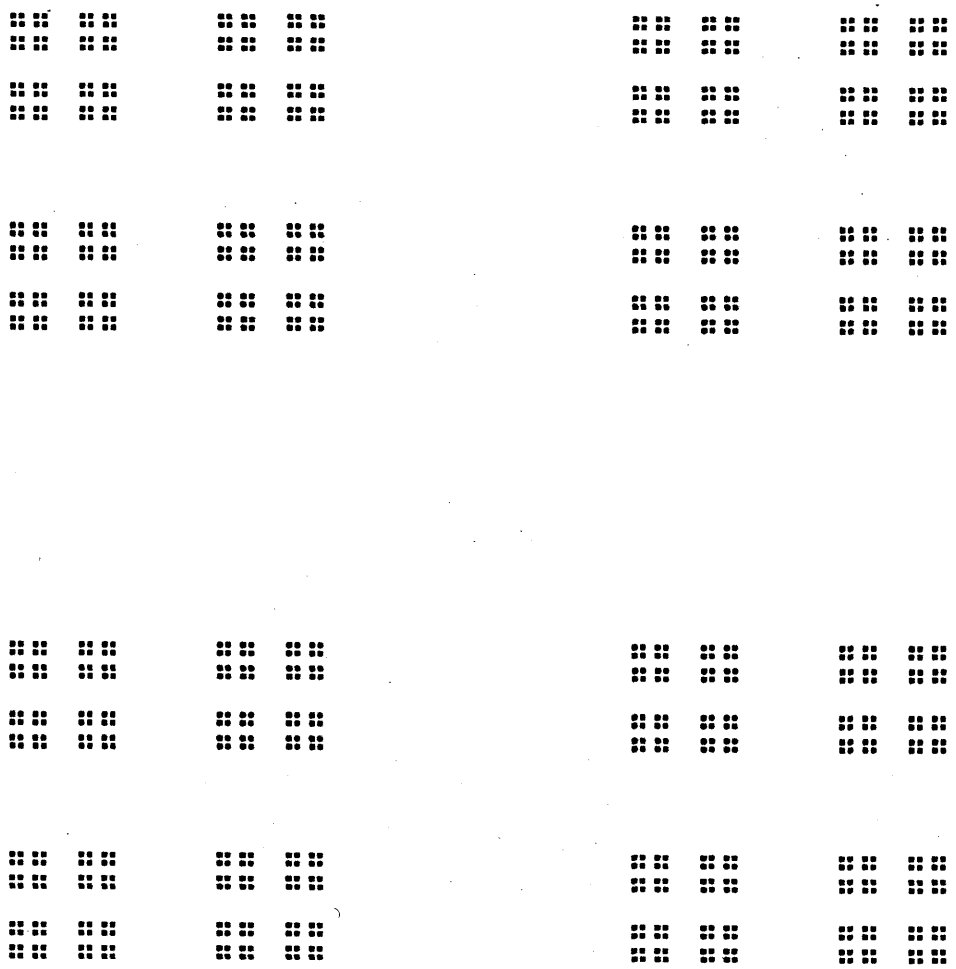

Figure 1.7: The Cartesian product of two sets X and Y, where X and Y are Cantor sets produces a two-dimensional fractal called the Cantor Dust

Chapter 2

Literature Review

2.1 Introduction

The behaviour of water has been pondered for centuries by natural scientists. It has been argued [27] that the application of experimental methods to studying fluids began with al-Biruni and al-Khazini in medieval period. Further progress was made by Pascal, Newton and d'Alembert and others, with classical mathematical studies of fluid mechanics culminating in the works of Stokes and Navier and the development of the Navier-Stokes (NS) equation (see equation 1.1) during the 1840's using conservation considerations and first-order approximations. These equations are non-linear; a property that results in their general insolubility.

One of the earliest treatments of particles diffusing in fluid was given by Taylor [28]. However, studies concerning the behaviour of inertial particles that are suspended in turbulent or random (which approximate turbulence) came much later. The contemporary field typically takes as its starting point a review paper by J. K. Eaton and J. R. Fessler in 1994 [29]. This paper highlights the basic properties of preferential concentration and argues that mechanism is common to a wide range of instances of particle clustering in fluid flows. The central importance of the Stokes number St is identified. It also highlights some previous models of preferential concentration, but finds them to be inadequate. This observation seeds much of the following work in particle clustering in turbulent flows.

2.2 Particles in Synthetic Turbulence

The first key paper of the early part of the 21st century is due to E. Balkovsky, G. Falkovich, and A. Fouxon in 2001 [30] which considers inertial particles that are suspended in a turbulent flow. It demonstrates that the distribution of the particles themselves can be conceived in terms of compressible flows, and highlights the importance that clustering has to a variety of physical and biological systems, most notably rain initiation in clouds.

In 2003, J.Bec published a paper entitled 'Fractal clustering of inertial particles in random flows'[31]. Two parameter are identified as being important for particle clustering, the Stokes number St and the β mass density ratio between fluid and particles. This paper is important for a number of reasons. Firstly, the fractal nature of the dynamical attractor upon which the particles sit is identified - this is important since it permits the use of Lyapunov exponent for its analysis. Secondly, the identification that maximal clustering occurs below $St \approx 1$. Finally the importance of understanding the multi-fractal properties of the dynamical attractor is identified. This permits Bec's follow up paper [32] in which a multi-fractal analysis is undertaken. It is important to remember that at this stage the particles considered are still collision-less 'ghost' particles. In this paper Bec highlights the distinction between two and three dimensional flows. In two dimensions clustering is observed for a range of dynamical parameters (St and β), a behaviour which is absent in three dimensions (the dimension of the attractor always remains above two). Following numerical simulations Bec identifies deviations from self-similar scaling in two dimensions.

Mehlig et al [33] in 2005 considered the trajectories of non-interacting particles suspended in a randomly moving fluid. The use of a random fluid to yield insight into turbulent flows is permissible largely due to Kolmogorov's 1941 theory - provided particles are below the Kolmogorov length scale of a turbulent flow then the flow can be treated as random. This paper expresses the maximal Lyapunov exponent, which dictates whether or not clustering will occur, as the expectation value of a random variable evolving under a stochastic differential equation. An asymptotic expansion for this Lyapunov exponent is developed in terms of a dimensionless measure of the inertia of the particles ϵ and a measure of the relative intensities of fluid velocity components. This allows the phase diagram of the system which has regions of 'coalescence' (regions where the particle density becomes very high) to be determined.

Bec et al [34] treat the mechanisms of preferential concentration and the sling effect coherently in order to estimate collision rates between inertial particles. Like Bec's previous work, preferential concentration is taken to be the convergence of trajectories toward a dynamically evolving attractor in phase space. However, collisions are neglected, allowing a Lagrangian dynamics approach to be adopted, and the collision rate between particles estimated in terms of the probability that two particles are closer than some distance r. Once again, maximal clustering is found when the Stokes number is of order unity.

Bec et al [15] 2006 also went onto consider the asymptotic limit of very heavy particles in turbulence by using the method employed by Mehlig et al [33] in which the two-particle dynamics is reduced to a non-linear system of three stochastic differential equations with additive noise. In two dimensions and the large Stokes number limit the probability distribution function of the longitudinal velocity difference between two particles is found to be given by a power law with exponent -3. This result is supported by numerical work.

The small Stokes number limit has also been considered. Wilkinson et al [35] produced an analytic result for the correlation dimension of the distribution of inertial particles in a random flow. The result is produced as a power series expansion in a small parameter which describes inertial effects. In 2007

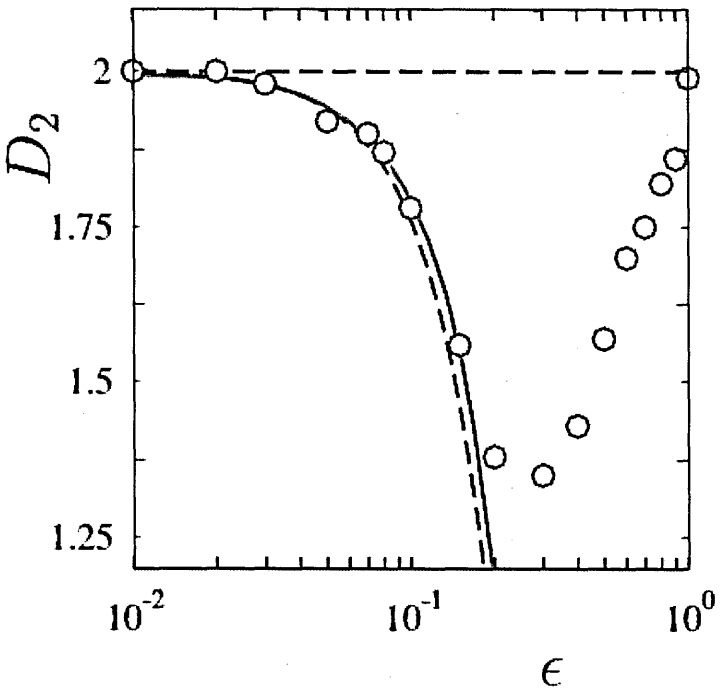

Figure 2.1: Adapted from [35]. Correlation dimension of particle distribution as a function of ϵ which is a small parameter which describes inertial effects. Each circle marks the point of numerical calculation of the correlation dimension, using very similar computational methods as used in this thesis. The solid line is the analytic result derived in the paper, and the dashed line a low order approximate form. It is interesting to note that the analytic solution does not capture the turning point at around $\epsilon = 1$

Bec and Chètrite [36] published a new model for the ejection of heavy particles from vortices based on a space-time discretisation of the dynamics. The model depends on two parameters: the fraction of space-time which rotating structures of the carrier flow occupy and the rate at which particles are ejected from them. It also gives the form of the PDF for the mass contained in a space-time cell.

The work of Fouxon [37] is important as it is explicitly calculates hydrodynamic forces between the inertial particles. Such interactions give a repulsion between particles and therefore smooths out the two particle correlation function, which in the case of ghost particles saturates. The effect is most pronounced around $St = 1$, where the attractor is densest.

Many papers invoke methods which utilise Lyapunov exponents to calculate physically significant properties of inertial particle distribution. Such concepts were exploited by Duncan et al in 2005 [38]. Here a divergent power series expansion is produced which was summed using Padé Borel summation (see the paper for details) to give an expression for the Lyapunov exponent in the limit of small viscous damping rate. They argue that 'Two distinct mechanisms compete (clustering onto fractal sets versus clustering onto caustics in an otherwise homogeneous background) and dominate in different regions

of the parameter space'.

In 2007 Wilkinson [39] analysed the clustering of inertial particles, which was termed 'unmixing' (to distinguish the clustered distribution of particles with inertia from the uniform scatter that results from inertia-less tracer particles) by calculating Lyapunov exponents.Padé Borel summation was used to show that the correlation dimension of resulting particle distribution agrees with previous results. The rate of caustic formation (see section 2.3) was also investigated. Wilkinson later [40] produced an expansion which showed that the first order correction in the Lyapunov exponent does not vanish, due to the observation that the particles do not sample the flow space ergodically.

2.3 Caustics

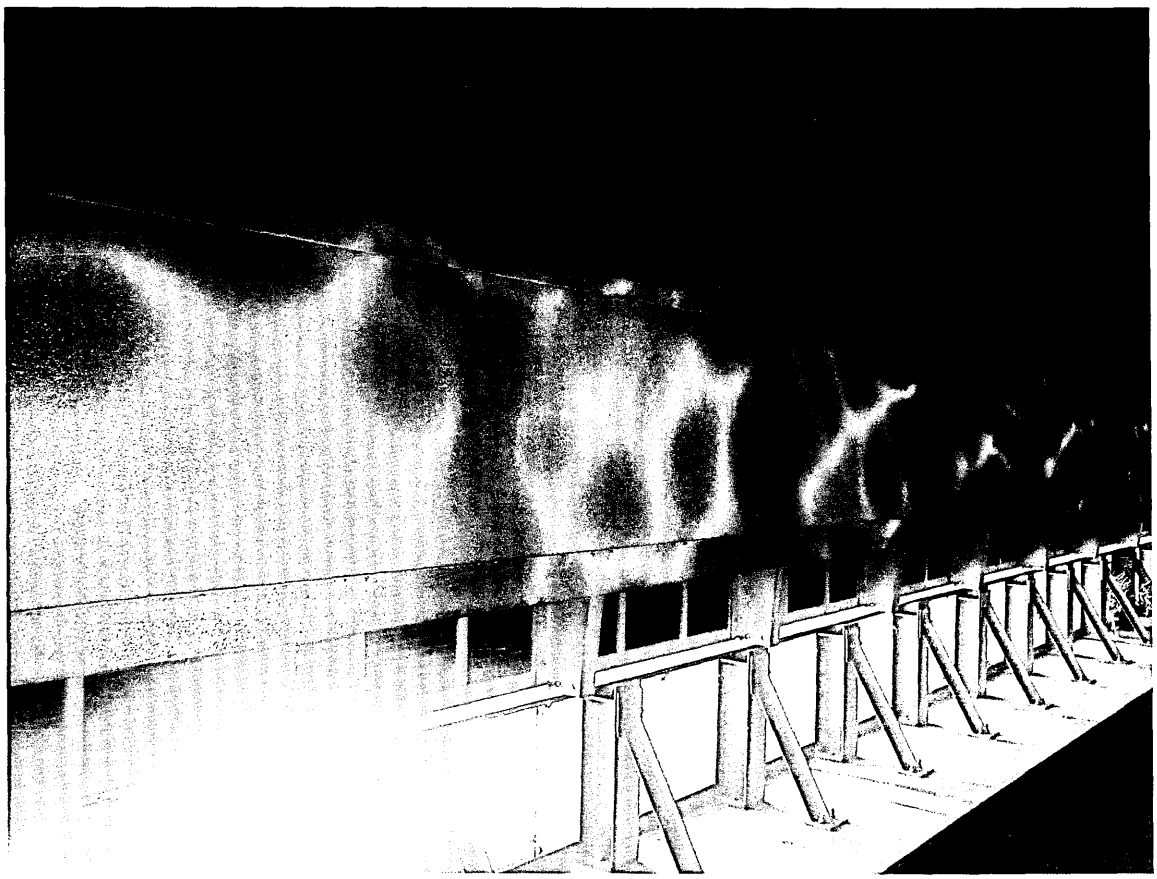

Figure 2.2: Caustics formed by light reflected from the surface of moving water onto the underside of a bridge. Caustic formation in the distribution of particles suspended in a randomly moving fluid is analogous.

When light refracts through surface of a gently undulating body of water onto the bottom a filamentary network of light patches is produced. This focusing effect corresponds to singularities in the electromagnetic field and was first identified by Berry [41]. In an analogous manner, when folding of the phase-space manifold occurs, caustics can form in the distribution of inertial particles in random flows. Wilkinson and Mehlig [42] gave the first description of caustic formation in the context of inertial particles by relating the evolution of the patterns to the Lyapunov exponents of the particle

trajectories. Caustics were also invoked by Bec et al in 2009 [43] in a study of collision rates of parti-

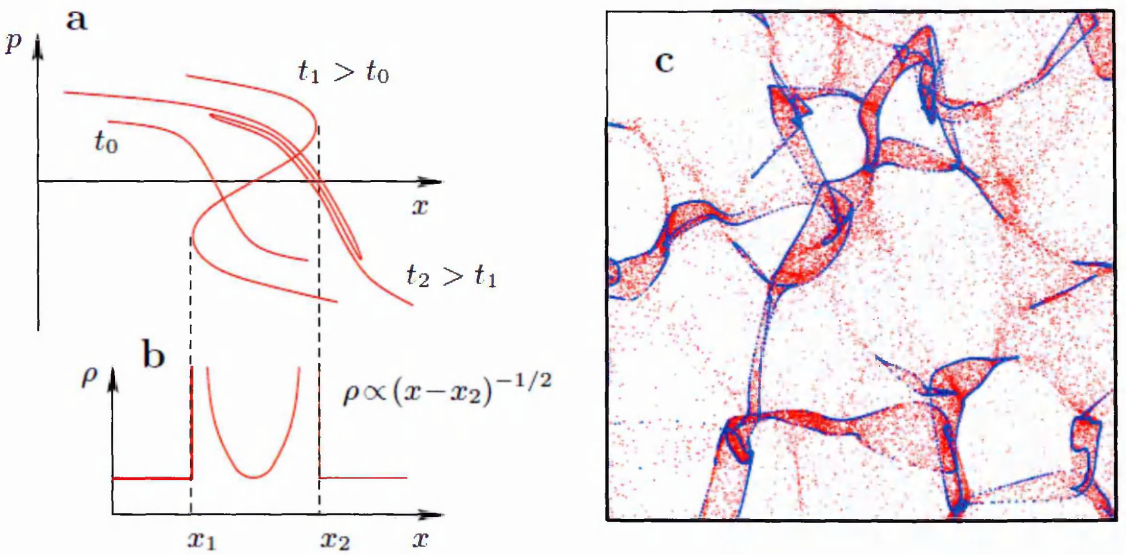

Figure 2.3: Adapted from [42]. Caustic formation is described by Wilkinson and Mehlig in the following way. (a) Particles are assumed to be distributed on a phase-space manifold, shown here as a phase curve in a one dimensional section. The phase curve develops folds (at time t_1), which become flattened due to the effect of damping (at t_2). (b) The particle density at time t_1 diverges on caustics, which are the projections of the folds. The caustics are created in pairs, with a high density of particles between each pair. (c) The particle distribution is shown in red, and the corresponding caustic curves are plotted as blue lines.'

cles. The authors discuss the relative importance of preferential concentration and caustic formation by examining DNS data.

2.4 DNS

Many papers have been written which collect data by DNS simulation [44, 45, 46]. The results provide as close to experimental data as is currently available, since particle tracking schemes are still in their infancy. Given the relatively large degree of specialisation required to reproduce DNS results, and the large computing power required DNS does not play any direct role in this thesis.

2.5 Other Papers of note

2.5.1 Inertial range

Several studies have been conducted regarding particles which are larger than the Kolmogorov length scale. In this region the flow of fully developed turbulence is self similar, a fact reflected in the studies undertaken. Unlike random fields (particles smaller than the Kolmogorov length scale) particles do not form fractal structures, but do still distribute in-homogeneously. [46, 15, 47]

2.5.2 Compressible flows

Falkovich et al [48] investigated inertial particles which are suspended in a fluid which is driven by telegraph noise. Telegraph noise is defined as a noise that switches randomly between two fixed values. Various appropriate limits are discussed by the authors and a phase diagram with a transition between aggregation and disorder identified. The paper also highlights the connections between inertial particles in random incompressible flows and non-inertial particles in compressible flows and suggests the link between the two phenomena is evident in the limit of small inertia, insofar as incompressible flows are approximated by tracers in a compressible field.

2.5.3 Segregation

Poly-disperse suspensions of inertial particles, i.e those for which a range of particles with different Stokes numbers are present, were examined in DNS simulations by Calzavarini et al [49]. They describe such flows in terms of 'segregation' between heavy and light particles by introducing indicator of segregation. From this indicator a length scale quantifying the degree of segregation of different types of particles is determined.

2.6 Granular gases

A related but independent area of study is that of the hydrodynamics of granular gases. The field considers the thermodynamic properties of interacting hard sphere (granular) material that is sufficiently rare to be modelled as a gas. The particles typically interact inelastically, and as such 'cooling' occurs. This is because it is possible to attribute an equivalent of thermodynamic temperature to such ensembles. A key author in this field has been Fouxon. Specifically, Fouxon and co-authors have written extensively on the formation of finite-time singularities (clustering) in such granular gases [50] [51].

Chapter 3

Spectal dimension of fractal sets

As discussed in section 1.3.1 the development of a definition of the fractal dimension of a set yields a great deal of information about the structure of the set under consideration. However, the fractal dimension yields no information regarding the isotropy of a fractal set. Indeed, two sets may have very similar fractal dimension but local structure that varies greatly. Figures 3.1 and 3.2 illustrate two different fractal point sets in two dimensions which have very similar correlation dimension, $D_2 \approx 1.73$ and $D_2 \approx 1.71$ respectively. However, as one examines the fine scale structure one notices that the points of the set shown in fig 3.1 accumulate on fine, anisotropic filaments whereas figure 3.2 is locally isotropic. This shows that information about the local isotropy of a set that is not present in the Renyi measure of fractal dimension itself. This chapter will consider one possible measure of the anisotropy of fractal sets. We develop a scheme which we demonstrate can distinguish between isotropic and non-isotropic sets. Moreover, the level of anisotropy is quantified in a dimension which we call the '*spectal*' dimension.

The sets illustrated in figures 3.1 and 3.2 are both point set fractals which result from two distinct models for physical processes. Figure 3.1 illustrates a model of light but not massless, neutrally buoyant particles which are suspended in a turbulent fluid flow. The inertia of the particles is sufficiently large to ensure that the particles are not simply advected (transported by the flow). As discussed in chapters 1 and 2, such particles are known to cluster [13] and that the attractor upon which their distribution converges is a fractal [52, 39]. The particle distribution is statistically isotropic, in that at a given point in space the time-averaged particle position will be uniform. However, at any given instant (such as that shown in 3.1) the particles can be seen to cluster on filamentary lines. This makes the local structure of the flow highly anisotropic, even though the global distribution is rotationally invariant. This behaviour occurs in general in attractors in low-dimensional dissipative dynamical systems, where the attractor has a local structure which is the Cartesian product of a line and a one-dimensional Cantor set [26].

The second example, figure 3.2 results from a model first described in [53] known as diffusion-limited

Figure 3.1: Distribution of particles with significant inertia moving in a two-dimensional incompressible velocity field (the equations of motion are specified in section 3.2). The particles tend to cluster and for the parameters used in this simulation (see section 3) the correlation dimension is $D_2 \approx 1.76$

aggregation (DLA). The DLA structure results from a system defined on a discrete two-dimensional lattice in which random walkers approach from infinity toward a central seed particle. When contact between the incoming particle and the cluster occurs, the walker sticks and another particle comes in from infinity. The process is repeated until the structure emerges (in this case 10^6 steps). Unlike the set shown in 3.1 the local structure of the DLA set cannot be approximated as a Cartesian product. Furthermore, a magnified subset of the DLA set does not appear anisotropic. Therefore, it is clear that two sets with very similar correlation dimensions may have markedly different isotropy characteristics. This difference in isotropy characteristics will have implications as to how the sets interact with light, this shall be explored more fully below.

3.0.1 Procedure

The following approach is used to characterise the local structure of a point set. First, take an element of the set and consider an ellipse centred on this point with its semi-minor axis of length ϵ and its semi-major axis of length $\delta = \epsilon^\alpha$, where $0 < \alpha < 1$. It is assumed that $\delta \ll \xi$ and $\epsilon \ll \xi$, where ξ is the characteristic lengthscale of the system below which fractal scaling is observable, and that $\epsilon \gg \epsilon_0$, where ϵ_0 is the lengthscale where the fractal scaling is limited by the finite number of points sampling the fractal measure. We then choose the orientation of the ellipse so that it maximises the number of other points which are contained within it. We denote the number of points under this optimally-oriented ellipse by $\mathcal{N}$. We repeat this for ellipses centred on other randomly selected points in the set, and compute the average value $\langle \mathcal{N} \rangle$ of the number of points which can be covered. In most

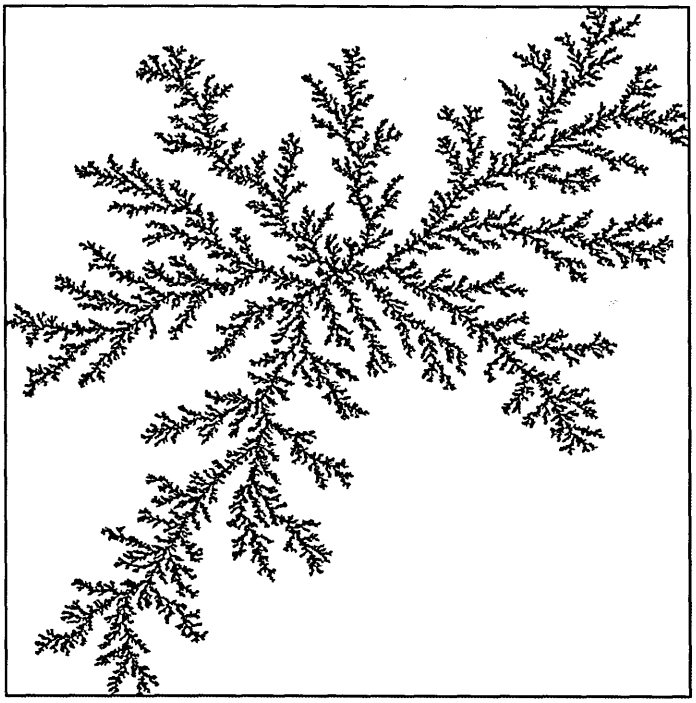

Figure 3.2: Distribution of particles determined by a diffusion-limited aggregation (DLA) process. This distribution has (approximately) the same fractal dimension as figure 3.1 $D_2 \approx 1.71$.

of the examples of point-set fractals which we investigated, the mean number of points in this ellipse is found to have a power law dependence:

$$\langle \mathcal{N}(\epsilon, \alpha) \rangle \sim \epsilon^{\beta(\alpha)} , \quad \delta = \epsilon^{\alpha} \tag{3.1}$$

where the exponent β depends upon α. In the case where $\alpha = 1$, the ellipse is a circle, so that this case reduces to a definition of the correlation dimension: $D_2 = \beta(1)$ (see the introduction and also [54]). In general β must decrease monotonically as α decreases since the area of the ellipse decreases. A diagram of the way in which size of the ellipses varies with α and ϵ can be seen in figure 3.3.

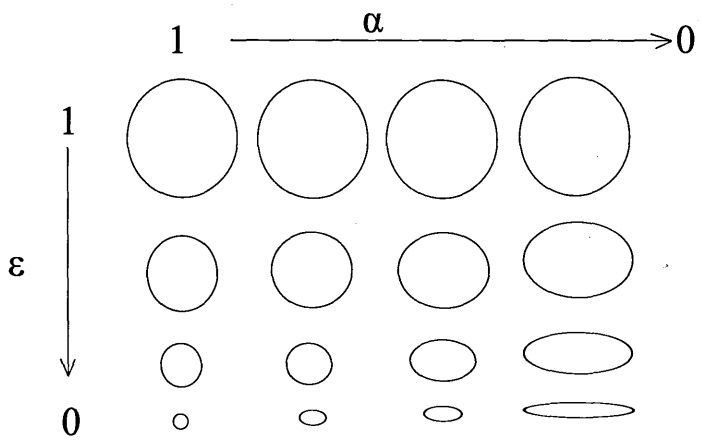

Figure 3.3: The above diagram shows how the size and shape of the ellipses used to cover the sets changes with α and ϵ

3.0.2 Partial dimensions

A related approach to the characterisation of fractal sets was proposed by Grassberger and colleagues [54], who considered covering a set (which is embedded in a d-dimensional space) with d-dimensional ellipsoids, with principal axes ϵ_i, ordered so that $\epsilon_1 > \epsilon_2 > \ldots > \epsilon_d$. Their work emphasises the case where the local structure of the fractal is a Cartesian product of sets, with dimensions ν_i, ordered so that $\nu_1 > \nu_2 > \ldots > \nu_d$. We hypothesise that the most efficient covering will occur when the ellipse is aligned with the direction of maximum density. Accordingly, the number of points covered is expected to satisfy

$$\langle \mathcal{N} \rangle \sim \epsilon^{\nu_1\epsilon_1+\nu_2\epsilon_2+\ldots+\nu_d\epsilon_d} \tag{3.2}$$

Examining the dependence of $\mathcal{N}$ upon the ϵ_i allows the *partial dimensions* ν_i to be determined.This approach is mentioned in several papers [54, 55, 56, 57], with the motivation to characterise a fractal set by means of its partial dimensions, ν_i, satisfying $\sum_{i=1}^{d} \nu_i = D_2$. These works do not prescribe how (or whether) the ratio $\epsilon_{i+1}/\epsilon_i$ approaches zero as $\epsilon_1 \to 0$. In our work this limiting behaviour is specified by the parameter α. Our numerical investigations encompass both fractal sets that have a Cartesian product structure, and those which do not.

3.0.3 S-Wave scattering

The physical motivation for considering the anisotropy structure has been alluded to, but we shall now examine this motivation more completely. It is known [58] that s-wave scattering of light from a fractal point set gives rise to an algebraic relation between the scattering wavelength k and the scattered intensity I, such that

$$I(k) \sim k^{-D_2} \ . \tag{3.3}$$

This relation arises from the fact that pair correlation scales as $g(r-r') \approx |r-r'|^{D-3}$ and the structure factor of electromagnetic radiation as $\int\int dr dr' g(r-r')e^{ikr}$. Certain complications can occur if the fractal is highly ordered as Detmann [59] points out, but these will not be directly addressed in this thesis. If the particles have a strong tendency to accumulate along lines in two dimensions (like the example shown in figure 3.1), or on planes in higher dimensions, light may scatter specularly[1] from these structures. Consider weak scattering of light with wavelength ϵ which propagates as a beam of width δ. When the path length for light scattered from different particles is large compared to ϵ, the scattering of light from $\mathcal{N}$ particles is incoherent, so that the contribution to the scattered intensity is $I \sim \mathcal{N}$. If, however, an ellipsoid of major axis δ and minor axis ϵ can be aligned to cover $\mathcal{N}$ particles, then there will exist directions where the path length is less than one wavelength, so that this set of $\mathcal{N}$ particles scatters light coherently (see figure 3.4). In these directions where the condition for specular reflection is satisfied by the optimal covering ellipsoid, there is a greatly increased intensity

[1] of or relating to the properties of a mirror, from the Latin speculris.

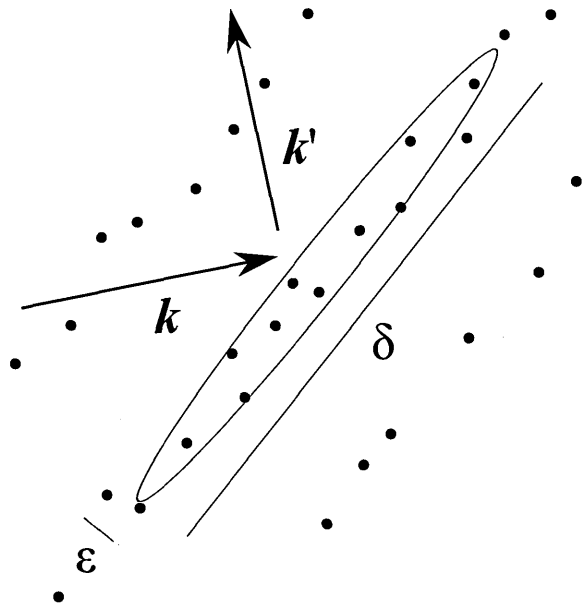

Figure 3.4: Scattering of a beam of light with wavenumber $\boldsymbol{k}$, width δ and wavelength ϵ: a cluster of $\mathcal{N}$ particles covered by an ϵ-δ ellipse scatters light coherently when the condition for specular reflection is satisfied. The wavevector $\boldsymbol{k}'$ satisfies the condition for specular reflection if the major axis of the ellipse is perpendicular to $\boldsymbol{k} - \boldsymbol{k}'$. In this case the scattered intensity from the particles under the cover is increased by a factor of $\mathcal{N}$.

$I \sim \mathcal{N}^2$. We coin the term spectal as a portmanteau of specular-fractal to indicate the degree to which anisotropy is present in a given fractal distribution. We investigate the dependence of the generalised dimension β upon the anisotropy exponent α. We show that the form of the function $\beta(\alpha)$ can distinguish between different fractal sets which have the same value of the correlation dimension $D_2 = \beta(1)$.

3.1 Some elementary estimates

3.1.1 Existence of the dimension

Before we proceed to numerical studies we consider some elementary estimates of the general form of $\beta(\alpha)$, defined by equation (3.1), we address the issue of whether the spectal dimension exists. When $\alpha = 1$, the exponent β coincides exactly with the correlation dimension of the set (see section 1.3.1). For other values of α, we do not know of any general argument which proves that the dependence of the optimal covering $\mathcal{N}$ has a power law relation to the size ϵ of the covering elements. For most of the point-set fractals which we examined we did find good numerical evidence that $\langle \mathcal{N} \rangle \sim \epsilon^{\beta}$ for small values of ϵ (extending down towards values of ϵ where the discrete sampling of the set becomes a limitation). Some interesting exceptions to this behaviour occurred in the case of inertial particles in a random flow, these will be discussed in section 3.2.

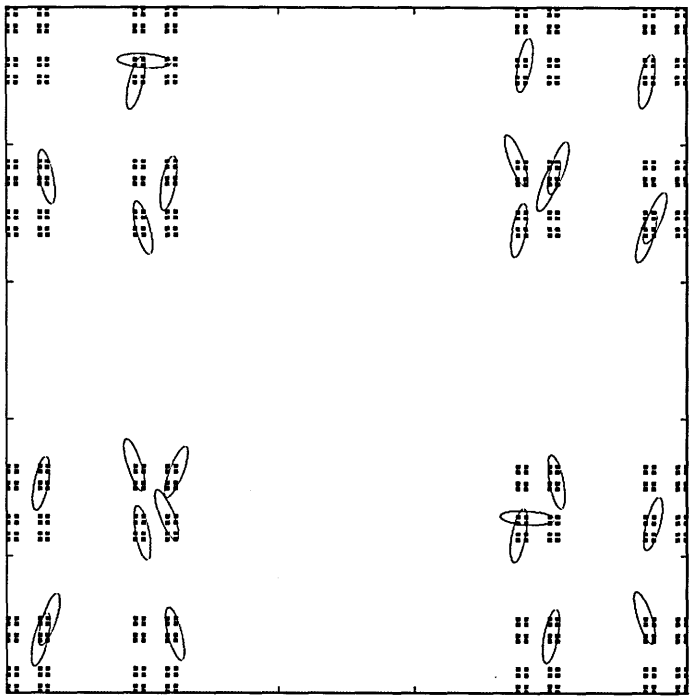

Figure 3.5: In the case where the fractal set is a Cartesian product of two Cantor sets, with dimensions D_x and D_y in the x and y directions, the optimal covering ellipse might be expected to have its major axis aligned with the direction corresponding to the denser set. In the case $D_y > D_x$, so the major axis of the ellipse would be expected to align with the y-axis. Here we illustrate a sample of the actual optimal covers, which have a distribution of angles of their principal axes.

3.1.2 Upper and lower bounds

Next we give an upper bound on $\beta(\alpha)$. Let us consider the expectation $\langle \mathcal{N} \rangle$ for the case where $\mathcal{N}$ does not depend on the orientation of the ellipse. The total number of particles in a disc of radius δ is proportional to δ^{D_2}, and if the set is locally isotropic then the coverage is independent of the orientation angle of the major axis of the ellipse, and a fraction ϵ/δ of these points lie within the ellipse. If we recall that $\delta = \epsilon^\alpha$ we have $\langle \mathcal{N} \rangle \sim \delta^{D_2-1}\epsilon \sim \epsilon^{1-\alpha+\alpha D_2} \equiv \epsilon^{\beta_+(\alpha)}$ for this isotropic fractal, so that

$$\beta_+(\alpha) = 1 + (D_2 - 1)\alpha \, . \tag{3.4}$$

is an upper bound on the exponent β. It is much harder to obtain a precise and non-trivial lower bound for $\beta(\alpha)$, but the following argument suggests a possible form for a lower bound. Consider the case where the fractal measure samples a Cartesian product (see section 1.3.3) of two one-dimensional Cantor sets of dimension D_x and D_y. We assume that $D_y \geq D_x$. Because the set is 'denser' in the direction of the y-axis, we expect that the optimal alignment of each ellipse is when its major axis is aligned with the y-axis (the same hypothesis was proposed in [54, 55]). The expected number of particles captured by a covering ellipse is then

$$\langle \mathcal{N} \rangle \sim \delta^{D_y}\epsilon^{D_x} = \epsilon^{\alpha D_y + D_x} \tag{3.5}$$

so that in the case where the fractal set is a Cartesian product, equation (3.5) implies that $\beta = \alpha D_y + D_x$. Now consider the smallest possible dimension which could be achieved according to this argument, if we allow the dimensions D_x, D_y of the component sets to vary so that $D_x + D_y = D_2$. The greatest number of particles in the ellipse, and hence the smallest dimension, is obtained by setting $D_y = 1$ and $D_x = D_2 - 1$. This gives a lower bound to the dimension for $D_2 \geq 1$ of the following form

$$\beta_{-}(\alpha) = D_2 - 1 + \alpha \, . \tag{3.6}$$

Since we do not consider sets of a dimension lower than 1 explicitly, this shall suffice.

The assumption that the covering ellipses align with the y-axis is not really correct, as evidenced by figure 3.5. It is plausible that the probability for an ellipses to be significantly mis-aligned decreases as $\epsilon \to 0$, but we were not able to obtain conclusive numerical evidence. We note that the argument leading to the proposed lower bound, $\beta_{-}(\alpha)$, is very similar to that presented in [54, 55] to motivate the concept of partial dimensions. Our numerical investigations, presented in section 3 below, will show that our proposed lower bound is a good starting point for discussion of $\beta(\alpha)$, but that the form of this function is non-universal.

3.2 Numerical investigations of dynamical fractals

The following section describes the numerical work done to calculate $\beta(\alpha)$ curves for the various fractals we consider. In terms of numerical techniques, we used FORTRAN carry out the calculations. The algorithms involved were of the 'brute force' approach, and did employ any novel techniques. A range of angles θ (through which the covering ellipses were rotated) was used, and robust results obtained using 30 values of θ, at equal rotation increments. Each set tested had a least 1 million points, a random sample of approximately 10% of these were chosen for each set and the average number of points contained for a given aspect of ellipse calculated. α was incremented at either 0.1 or 0.05 depending on the rate of change of $\beta(\alpha)$ for a given fractal (again robustness of the results was checked). For the deterministic Sierpinski fractals (see below) typically 7-10 generations of the fractal were used in the first instance, this was then increased to ensure that the results did not change for 'deeper' approximations to the underlying fractal. A maximum of 12 generations were employed. Each fractal took around 10 hours of computer time to analyse, but the cluster allowed for several instances to be computed simultaneously, dramatically speeding up the results. For the inertial particles model the simulation was run for sufficiently long to ensure that transient behaviour had died down. The longest calculation (of an extremely dense inertial particle set) took 14 days to complete.

3.2.1 Particles in a random flow

Now we consider the numerical investigation of the fractals illustrated in figures 3.1 and 3.2 respectively. Figure 3.1 illustrates the distribution of independently moving inertial particles in a random velocity field. As mentioned in chapters 1 and 2 the equations of motion for the position of a given particle are [13]

$$\dot{\boldsymbol{r}} = \boldsymbol{v} \ , \quad \dot{\boldsymbol{v}} = -\gamma[\boldsymbol{v} - \boldsymbol{u}(\boldsymbol{r}(t), t)] \tag{3.7}$$

where γ is the rate at which the particles relax towards the fluid velocity, and where $\boldsymbol{u}(\boldsymbol{r}, t)$ is a randomly fluctuating velocity field satisfying the condition for incompressibility; $\boldsymbol{\nabla} \cdot \boldsymbol{u} = 0$. Particles in the fluid flow cluster if the damping timescale γ^{-1} is comparable to a timescale characterising the velocity field. We used a random vector field with a very small correlation time, using the same definitions as in [35], where the importance of inertial effects is characterised by a dimensionless parameter, which was referred to as ε in that work, but which is denoted by η here. It is defined in terms of the correlation function of the velocity gradient experienced by a particle with trajectory $\boldsymbol{r}(t)$:

$$\eta^2 = \frac{1}{2\gamma} \int_{-\infty}^{\infty} \mathrm{d}t \ \left\langle \left(\frac{\partial u_x}{\partial x} \right) (\boldsymbol{r}(t), t) \left(\frac{\partial u_x}{\partial x} \right) (\boldsymbol{0}, 0) \right\rangle \tag{3.8}$$

In figure 3.1, we showed a realisation of the long-time dynamics. The velocity is periodic on the unit square, and was generated from a stream function with correlation function $\psi(\boldsymbol{r}, t)$ with statistics $\langle \psi(\boldsymbol{r}, t) \rangle = 0$, $\langle \psi(\boldsymbol{r}, t) \psi(\boldsymbol{0}, 0) \rangle = A^2 \exp(-|(r)|^2 / 2\xi^2) \exp(-t/\tau)$, with $\xi = 0.2$, τ small and A chosen such that $\eta = 0.1$. The correlation dimension for this value of η is $D_2 \approx 1.76$ [35].

We examined whether the mean value of the optimal covering number, $\langle \mathcal{N} \rangle$, shows a power law dependence upon ϵ. The data shown in figure 3.6 show a good fit to a power law, for values of α as low as 0.2. At very small values of α, the area of the ellipses decreases very rapidly as $\epsilon \to 0$, so that the values of $\langle \mathcal{N} \rangle$ become too small to give reliable results.

The program that was used in this thesis was written by Professor Michael Wilkinson. It works by calculating the velocity field which modifies initially stationary particles, as they are moved by the flow. The amount by which their motion is effected depends on a random number (generated using the same algorithm as mentioned above) which is added to the Fourier components of the particles velocity. The program was modified to output the particle positions at each timestep (or every 5 timesteps) to allow the correlation dimension to be determined.

There were a small number of cases where we found that the covering data were not well fitted by a power law in ϵ. These were confined to the inertial particles model, for small values of α and for values of η where the value of D_2 is close to its minimum, which is $D_2 \approx 1.35$ at $\eta \approx 0.7$. Figure 3.7 illustrates the case where the fit to a power law was the least good. We were unable to give an explanation for this phenomenon, but perhaps the effect is due to the presence of caustics, or other complex multifractal effects.

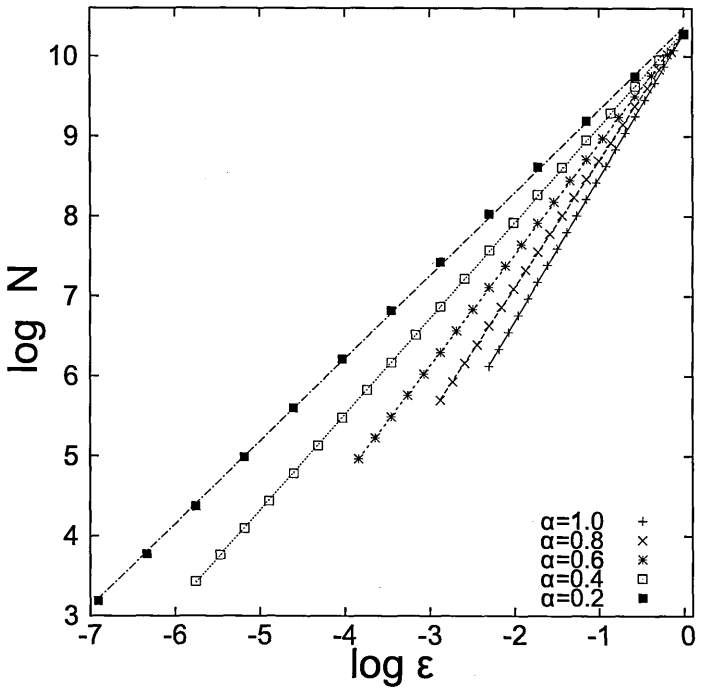

Figure 3.6: The mean number of points in an optimal cover, $\langle \mathcal{N} \rangle$ as a function of ϵ, for various values of α. The slope increases monotonically with α, which ranges from $\alpha = 0.2$ to $\alpha = 1$ in increments of 0.1. These data, for the random flow model with $\eta = 0.5$, show excellent fits to a power law over a wide range of ϵ. A comparable quality of fit was found in all of the other data.

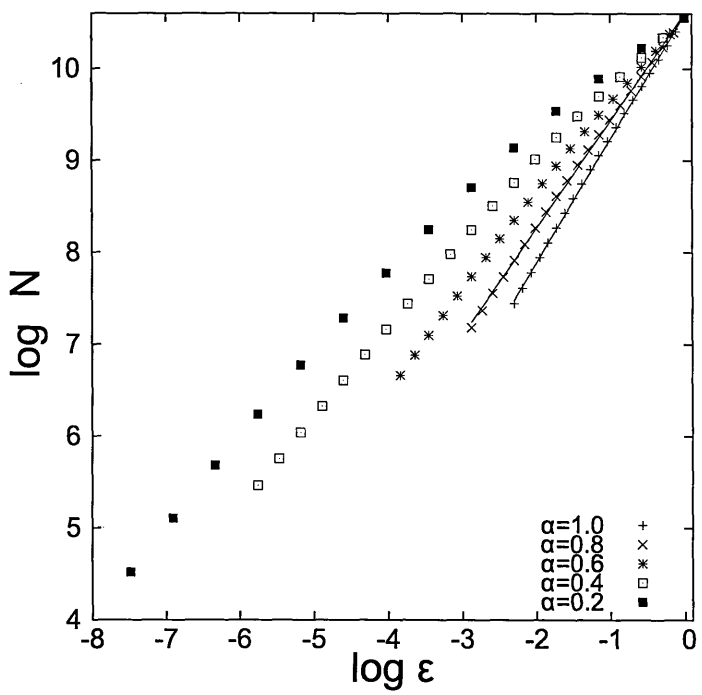

Figure 3.7: Same as figure 3.6, except $\eta = 0.7$, where $D_2 \approx 1.35$. In this case the covering data are not a good fit to a power law in ϵ for $\alpha \leq 0.3$.

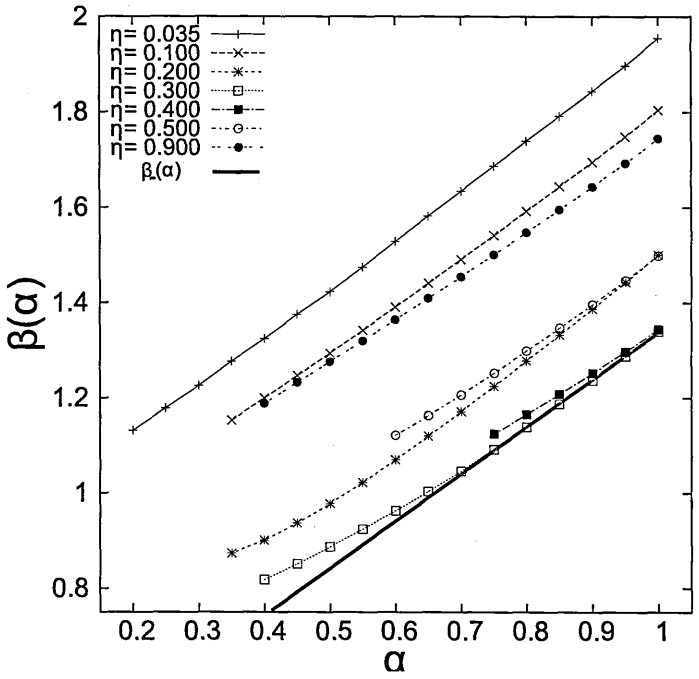

Figure 3.8: $\beta(\alpha)$ for inertial particles in a random velocity field, using a model defined in [35]. The curves are labelled according to the parameter η which quantifies the importance of particle inertia. The sold red line illustrates $\beta_{-}(\alpha)$ for $\eta = 0.4$ and $\eta = 0.3$, other $\beta_{-}(\alpha)$ lines are parallel to this one, passing through D_2.

In figure 3.8 we show the $\beta(\alpha)$ for this systems at several different values of the inertial parameter η. Fractal attractors of dynamical systems typically have a local structure which is a Cartesian product of a Cantor set and a line due to the stretching and folding of the phase space (see 1.3.3). Following the discussion in section 3.1 we therefore expect that the exponent $\beta(\alpha)$ should be given by equation (3.6), that is $\beta(\alpha) \approx \beta_{-}(\alpha)$. We find, however, that $\beta_{-}(\alpha)$ is not a very good approximation, and figure 3.8 shows that different $\beta(\alpha)$ curves may be obtained for cases with the same fractal dimension.

3.2.2 DLA

We also investigated $\beta(\alpha)$ for fractals generated by DLA, one realisation of which is illustrated in figure 3.2. The data for particle positions were simulated by Dr Michael Morgan of the University of Seattle. In the case of isotropic diffusion, the correlation dimension of the resulting cluster is $D_2 \approx 1.71$. The values of the slopes β extracted from least-squares fits similar to those in figure 3.6 are plotted in figure 3.9 as a function of α.

3.3 Sierpinski substitution fractals

The examples that we considered in section 3.2 are both multi-fractal sets, and it is desirable to investigate $\beta(\alpha)$ for a model which is a simple fractal, avoiding the complications that arise when dealing with multi-fractal sets [60]. Here we construct a class of generalisations of the Sierpinski carpet, which are simple fractals rather than multi-fractal measures. The construction that we use

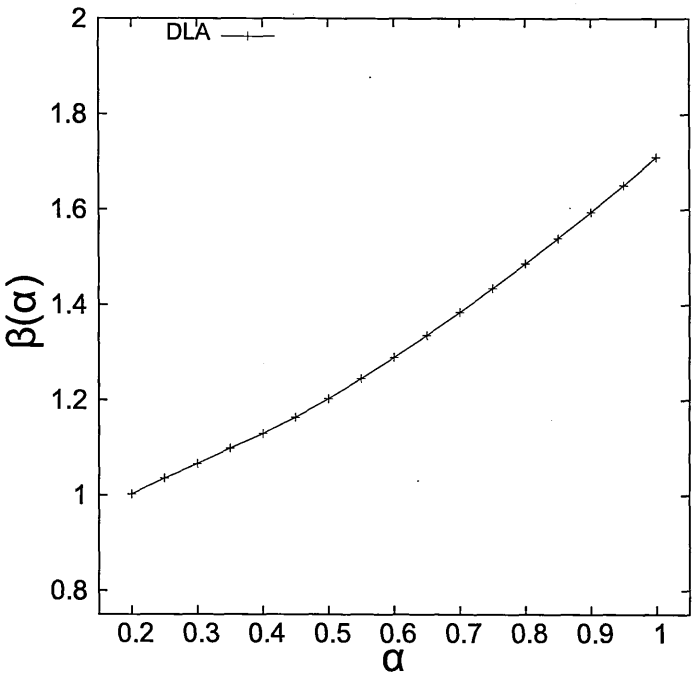

Figure 3.9: $\beta(\alpha)$ for a diffusion limited aggregation (DLA) cluster. The curves function as a guide for the eye.

is closely related to one proposed independently by Bedford [61] and McMullen [62]. We show that different elements from this class of sets can have different $\beta(\alpha)$ functions despite having precisely the same value of $D_2 = \beta(1)$.

We generate an approximation to a fractal set by a hierarchical process consisting of n generations. We generate a set of M^n points, where M is an integer, as follows. The points $\boldsymbol{x}_k$ lie in the unit square $[0,1] \otimes [0,1]$, and have coordinates of the form $(x_i, y_i) = (i/N_1^n, j/N_2^n)$, where N_1, N_2 are positive integers satisfying $N_1 N_2 > M$.

We define a 'masking matrix' $\mathbf{F}$ with elements F_{ij} as an $N_1 \times N_2$ matrix which has elements which are either 1 or 0, and we let M be the number of non-zero elements of $\mathbf{F}$. We construct the model set by the following recursive construction. First consider the 'first generation' set of M points $\boldsymbol{x}_k$, labelled by an index $= 1 \ldots M$, where a point is placed at $((i-1)/N_1, (j-1)/N_2)$ if $F_{ij} = 1$. At the next generation *each* of these points is replaced by a set of M points, based on a lattice with spacings N_1^{-2} and N_2^{-2} in the x and y directions respectively, which are selected by the criterion that $F_{ij} = 1$. In general, after n generations each point $\boldsymbol{x}_k$ is replaced by M points with positions $\boldsymbol{x}_{k'}$, where k' is an index of the $(N_1 N_2)^{n+1}$ points, with positions

$$\boldsymbol{x}'_{k'} = \boldsymbol{x}_k + \left(\frac{i-1}{N_1^{n+1}}, \frac{j-1}{N_2^{n+1}} \right) . \tag{3.9}$$

A point labelled by (i,j) added to the set if and only if $F_{ij} = 1$.

As an example, consider the case where $N_1 = N_2 = 3$ and where $F_{22} = 0$ is the only element of $\mathbf{F}$ which is equal to zero, so that $M = 8$. Iterating this construction gives a version of the

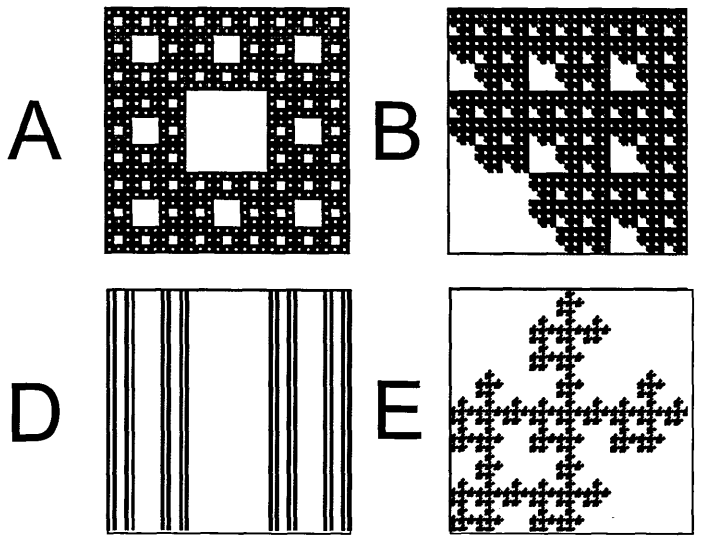

Figure 3.10: Examples of fractal sets generated by the construction defined in section 4. In all of these examples, $N_1 = N_2 = 3$. The Cantor set is then defined by listing the zero elements of the masking matrix: (**a**) $F_{22} = 0$, $D_q = \ln 8/\ln 3$, (**b**) $F_{13} = 0$, $D_q = \ln 8/\ln 3$, (**d**) $F_{21} = F_{22} = F_{23} = 0$, $D_q = \ln 6/\ln 3$, (**e**) $F_{13} = F_{31} = F_{33} = 0$, $D_q = \ln 6/\ln 3$. The lettering corresponds to figure 3.12

Sierpinski carpet set, illustrated in figure 3.10(**a**), with dimension $D_q = \ln 8/\ln 3$. By varying the zero elements of the masking matrix, we can generate many other Cantor sets, some examples of which are illustrated in the other panels of figure 3.10. The resulting sets are clearly simple fractals (as opposed to multifractals, hence D_q is the same for all values of q, hereafter we drop the subscript q). By making other choices of the masking matrix we can construct other Cantor sets with dimension

$$D = \frac{2 \ln M}{\ln (N_1 N_2)} \, . \tag{3.10}$$

This construction allows us to create distinct fractal sets with exactly the same dimension, such as in panels (**a**) and (**b**) or panels (**c**) and (**d**) of figure 3.10. Moreover, by a suitable choice of the masking matrix, we can generate fractal sets which are Cartesian products (such as figure 3.10(**d**)), as well as those which are not (such as figures 3.10(**a-c**)). The routine specific to initialising the procedure in section 3.0.1 for determining $\beta(\alpha)$ of these sets was not complex. To generate the fractals, two large arrays, for the x and y dimension, were generated (of 10 million blocks each), and each point tested for each generation of the fractal to see if it lies within the fractal specified by the masking matrix. The number of generations was picked to ensure that each fractal had at least a million points (this was discovered to be a robust number to do the calculations with), so for a single deletion fractal (**A** or **B** in 3.12) 7 generations yields $8^8 = 2,097,152$ points). Next, the ellipses were generated for a range of α values and a random subset of points chosen (using an off-the-shelf FORTRAN random number generator). Each ellipse is rotated about the selected point a simple test to discover the optimal orientation carried out using IF statements. Tests to check that the ellipses do not intersect the outer boundary of the fractal are also undertaken for each selected point. Once the number of

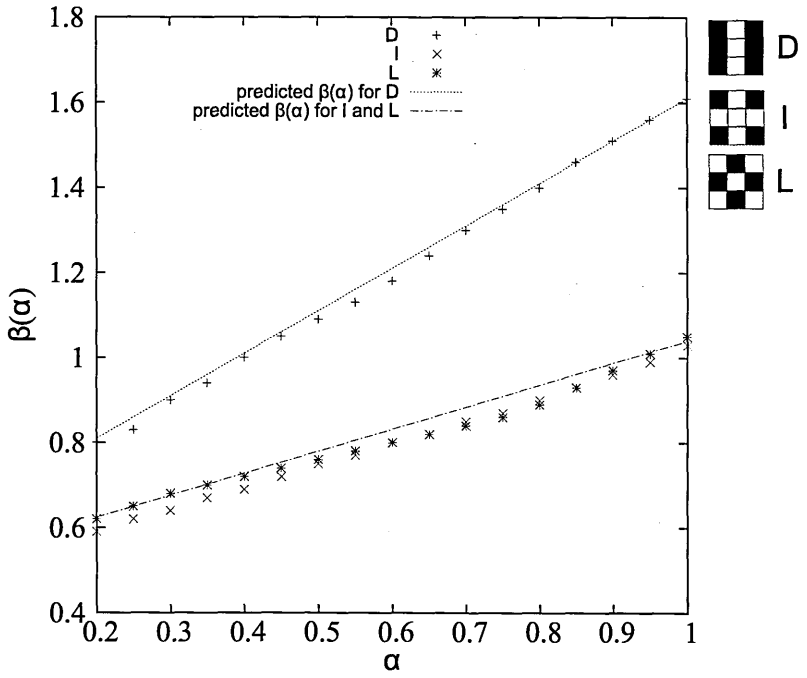

Figure 3.11: $\beta(\alpha)$ for the generalised Sierpinski model for masking matrices of non-trivial cartesian product sets **D**,**I**,and **L** with the respective estimates for their $\beta(\alpha)$ curves.

points in each selected ellipse is determined this is added to an averaging array, which then provides the value from which the gradient, $\beta(\alpha)$ is calculated. We investigated the function $\beta(\alpha)$ for sets which are produced by this generalised Sierpinski construction. The results are illustrated in figure 3.12, for seventeen sets produced using a 3×3 masking matrix. The key at the right hand side of the figure indicates the pattern of deletions in the masking matrix, ordered by the number of deleted points.

First we discuss those sets which are a Cartesian product. These include examples **D**, **I**, **L**, **P** and **Q** in figure 3.12. The simplest example is set (**d**) in figure 3.10, which is also example **D** in figure 3.12. For this set, equation (3.6) predicts that $\beta(\alpha) = D - 1 + \alpha$, which shows excellent agreement with figure 3.12. By setting $N_1 = N_2 = 3$ and $F_{12} = F_{21} = F_{23} = F_{32} = F_{22} = 0$ we produce a set with dimension $D = \ln 4/\ln 3 = 2\ln 2/\ln 3$, which is a Cartesian product of two Cantor sets of dimension $D_x = D_y = D/2 = \ln 2/\ln 3$. This is example **I** in figure 3.12. Example **L** is closely related: this set is similar to example **I**, rotated by $\pi/4$. These data show quite poor agreement with the prediction from equation (3.5), from which we expect $\beta(\alpha) = D(1+\alpha)/2$ (but good agreement with each other). This is probably because this is a degenerate case, where $D_x = D_y$, whereas the argument used to obtain (3.6) assumes that $D_y > D_x$. The other two examples in figure 3.12 which are Cartesian products very simple: **P** is a Cartesian product of a line and a point, and **Q** is the product of a Cantor set of dimension $\ln 2/\ln 3$ and a point. For these examples there is excellent agreement with the predictions of equations (3.5) and (3.6), which indicate straight lines of slope unity and $\ln 2/\ln 3$ respectively. We also investigated an example which is a Cartesian product of two Cantor sets with different dimensions, namely $N_1 = 4$, $N_2 = 3$, with non-zero elements $F_{11} = F_{13} = F_{41} = F_{43} = 1$

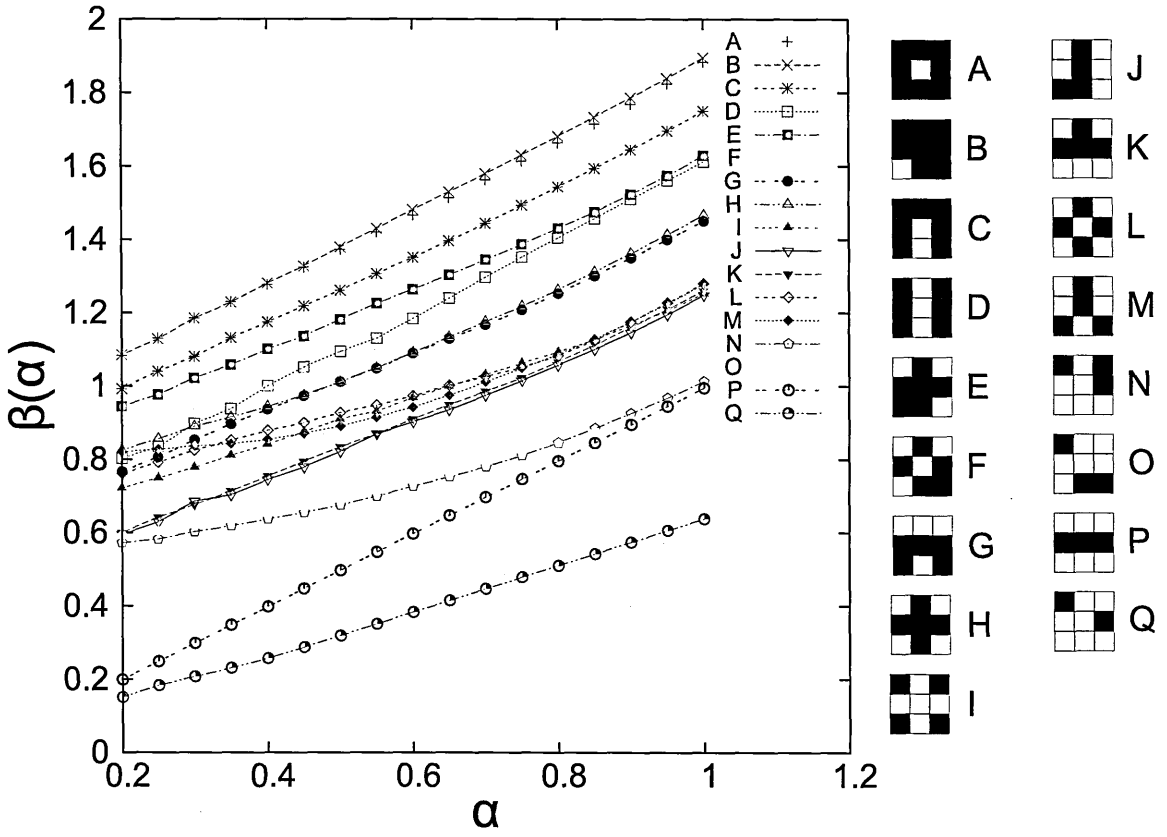

Figure 3.12: $\beta(\alpha)$ for the generalised Sierpinski model.The curves are labelled by a key giving the zero elements of the masking matrix.

(which is the set illustrated in figure 3.5). This is the Cartesian product of two one-dimensional Cantor sets with dimensions $D_x = \frac{1}{2}$ and $D_y = \ln 2/\ln 3$. We find that for this set the generalised dimension is $\beta(\alpha) = D_x + \alpha D_y$, also in agreement with (3.5). We show $\beta(\alpha)$ in 3.11 for the non-trivial cases, along with respective predicted form.

We also investigated $\beta(\alpha)$ in cases where the set is not a Cartesian product. These differ from the data for the Cartesian product sets. They can be organised into sets which have apparently identical $\beta(\alpha)$ curves. In most of the cases examined in figure 3.12, all of the sets which have the same value of M (and hence of D_2) have $\beta(\alpha)$ curves which are identical, to within numerical fluctuations. Examples of such groups are $(M = 8 : \mathbf{A}, \mathbf{B})$, $(M = 5 : \mathbf{G}, \mathbf{F})$, $(M = 4 : \mathbf{J}, \mathbf{K})$, $(M = 3 : \mathbf{N}, \mathbf{O})$. We show these cases in figures 3.13 and 3.14 for clarity. Note, however, that for $M = 4$, set $\mathbf{M}$ is not a Cartesian product and yet is clearly different from $\mathbf{J}$ and $\mathbf{K}$. One notable feature of all of these examples is that the slope of $\beta(\alpha)$ is close to unity at $\alpha = 1$. This feature is shared by the random flow and DLA data.

3.4 Summary

This investigation is the first systematic study of fractals using a cover set which becomes more anisotropic as it is made smaller. We characterised the efficiency of covering by a generalised dimension

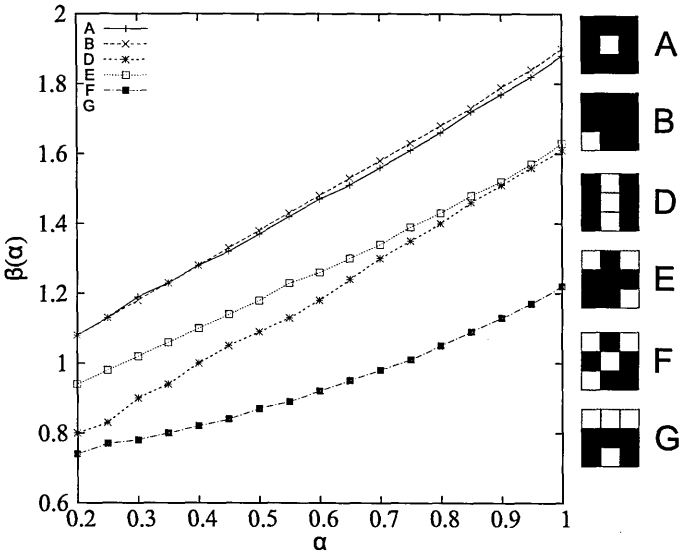

Figure 3.13: $\beta(\alpha)$ for the generalised Sierpinski model for masking matrices **A**,**B**,,**D**,**E**,**F** and **G**. We argue that the difference between **D** and **E** are due to the different isotropy properties of the sets. The same difference is seen in **F** and **G**.

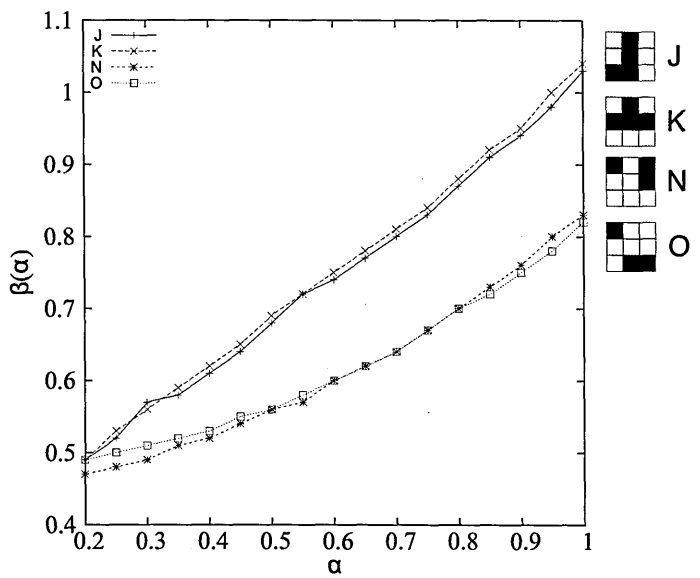

Figure 3.14: $\beta(\alpha)$ for the generalised Sierpinski model for masking matrices **J**,**K**,**N** and **O**.

$\beta(\alpha)$. We found that different sets with the same correlation dimension D_2 can have different $\beta(\alpha)$.

In the case where the fractal is locally a Cartesian product of a line and a Cantor set, a heuristic argument (similar to that given in [54] and subsequent papers) suggest that $\beta(\alpha)$ should be given by (3.6). We find that this expression works well for simple model sets of the type considered in section 4. In the case of clustering of inertial particles, however, we find that equation (3.6) does not give a good approximation to $\beta(\alpha)$.

In three or more dimensions there may also be a tendency for particles to accumulate on filamentary structures, as well as on planes. This could be characterised by defining the exponent β as a function of two parameters, α_1, α_2 defining a covering ellipsoid with principal axes ϵ, ϵ^{α_1} and ϵ^{α_2}. Studies of this kind would constitute a larger study, but be essential for understanding the interaction of light with complex fractal structures.

Chapter 4

A Model For Alignment Between Microscopic Rods And Vorticity

We have seen in the previous chapter that complex fractal structures result from inertial particles in a random velocity field. In the following chapter we consider a different but related situation. Instead of considering particles which are modelled as points we take the suspended particles to be elliptical, rod like particles. The outcome of the work is an exactly solvable analytic model for the alignment of the rods with the flow (the exact parameters of which shall be described in more detail below). The analytic model for the rod alignment is compared to numerical simulations, and very strong agreement established. Questions regarding the orientation of microscopic rods in random flows have relevance in several industrial applications, most notably in paper production.

4.1 Introduction

Microscopic rod-like bodies suspended in a fluid flow rotate in response to the velocity gradient of the flow. This degree to which particles align can influence the optical or rheological properties of the suspension. The equation of motion for the orientation of microscopic ellipsoidal particles was obtained by Jeffery [63]. The implications of this equation of motion for the orientation have been considered by numerous authors: for example [64] discusses the motion of general axisymmetric particles, [65] considers the role of Brownian motion, [66] discuss the alignment fields in (respectively) regular and chaotic flows, and [67, 68] are experimental contributions. There are, however, still aspects which are not thoroughly understood. One surprising observation based on DNS studies of Navier-Stokes turbulence is that in isotropic fully-developed turbulence, rod-like particles show significant alignment with the vorticity vector, but negligible alignment with the principal strain axis [69]. This was given a qualitative explanation in [69], but it is desirable to have a model for this surprising effect which can be analysed quantitatively. This chapter considers an exactly solvable model for the

alignment of rods with vorticity. The formulation of this model was motivated by observations about the velocity gradient field of turbulence. It has been observed that the fluctuations of the vorticity vector decay much more slowly than fluctuations of the rate of strain: [69] shows evidence that the correlation functions of strain and vorticity both show approximately exponential decay, with decay times $\tau_s \approx 2.3\tau_K$ and $\tau_v \approx 7.2\tau_K$ respectively, where τ_K is the Kolmogorov timescale of the turbulence (see 4.1). Similar results were reported earlier by Girimaji and Pope [70] and Brunk, Koch and Lion [71]. This observation suggests that it may be helpful to consider the limit as $\tau_v \to \infty$, that is the limit where the vorticity is frozen, in order to explain the observed alignment. We use an Ornstein-Uhlenbeck process to model fluctuations of the velocity gradient, and consider the limit where the vorticity evolves very slowly. This model is solved exactly in the limit where the strain which occurs over the timescale τ_s is small. The alignment of the rod direction $\mathbf{n}$ and the direction of the vorticity vector $\mathbf{e}_\omega$ can be described by computing the probability density function (PDF) of $z = \mathbf{n} \cdot \mathbf{e}_\omega$. We find that in these limits the PDF of z, denoted by $P(z)$, can be computed exactly. This analytically solvable model has a single dimensionless parameter, $\zeta \equiv \omega\tau_s$, where ω is the angular velocity of rotation about the vorticity vector. We find that when $\zeta \gg 1$, the probability density has two sharp peaks, one at $z = \pm 1$ (indicating perfect alignment with vorticity), the other at $z = 0$ (implying that the rods are perpendicular to the vorticity). In the limit as $\zeta \to \infty$, the peak at $z = \pm 1$ is higher than at $z = 0$, but it is also narrower, with both peaks containing a finite probability. Section 4.2 discusses the model which will be solved: the equations of motion for a microscopic rod are considered in section 4.2.1, and the Ornstein-Uhlenbeck model for the velocity gradient of an isotropic random flow is described in section 4.2.2. Section 4.3 discusses a transformation of the equation of motion in which the *isotropic* velocity gradient is replaced by a pure strain field which is *axisymmetric* about the direction of the vorticity vector, and it discusses the parametrisation of such axisymmetric random strain fields. Section 4.4 considers the general solution for alignment of rod-like particles in axisymmetric strain fields, before specialising to the solution of the model developed in section 4.3. Section 4.5 summarises our conclusions. The analysis in section 4.4 is closely related to recent work by Vincenzi [72], who analysed the alignment of ellipsoidal particles in an axisymmetric Krainchnan-Batchelor model.

4.2 Equations of motion

4.2.1 Non-linear and linear equations of motion for rods

In 1922 Jeffrey obtained the equation of motion of microscopic rod-like particles in the velocity gradient that results from fluid flow by extending earlier work by Einstein. We consider microscopic objects advected in a fluid with velocity field $\boldsymbol{u}(\boldsymbol{r}, t)$. The objects are assumed to be neutrally buoyant, and smaller than any lengthscale characterising the fluid, but sufficiently large that their Brownian motion

need not be considered. A specific instance of this kind of physical situation would ice-crystals in clouds, they are too large for Brownian motion have an effect, but smaller than the typical length scale of turbulence in the upper atmosphere (see [2] for more information). The motion of the body is described by the position of its centre, $\boldsymbol{r}(t)$, and the direction of a unit vector aligned with its axis, $\mathbf{n}(t)$. The centre of the body is assumed to be advected by the fluid flow: $\dot{\boldsymbol{r}} = \boldsymbol{u}(\boldsymbol{r}, t)$. The motion of the unit vector $\mathbf{n}$ defining the axis of symmetry is determined by elements of the velocity gradient tensor, evaluated at the centre of the body:

$$A_{ij}(t) = \frac{\partial u_i}{\partial r_j}(\boldsymbol{r}(t), t) \tag{4.1}$$

where $\boldsymbol{r}(t)$ is the advected particle trajectory. As mentioned above, the equation of motion of the *director vector* of a microscopic rod-like body is [63]

$$\frac{\mathrm{d}\mathbf{n}}{\mathrm{d}t} = \mathbf{A}(t)\mathbf{n} - (\mathbf{n} \cdot \mathbf{A}(t)\mathbf{n})\mathbf{n} \,. \tag{4.2}$$

We assume the flow is incompressible, so that $\sum_{i=1}^{3} A_{ii} = 0$. This tensor can be decomposed into a symmetric part $\mathbf{S}$, which is termed the strain rate, and an antisymmetric part $\boldsymbol{\Omega}$, which is the vorticity tensor:

$$\mathbf{A} = \mathbf{S} + \boldsymbol{\Omega} \,, \quad \mathbf{S}^{\mathrm{T}} = \mathbf{S} \,, \quad \boldsymbol{\Omega}^{\mathrm{T}} = -\boldsymbol{\Omega} \,. \tag{4.3}$$

If the velocity gradient matrix were constant in time, the equation of motion (4.2) would imply that the vector $\mathbf{n}$ would become aligned with the eigenvector corresponding to its largest eigenvalue. However, numerical simulations of equation (4.2) for velocity fields of fully developed turbulence show a different, and unexpected, phenomenon [69]. It is found that the direction vector $\mathbf{n}$ has negligible correlation with the dominant strain eigenvector, but that it does have a quite pronounced correlation with the vorticity vector, $\boldsymbol{\omega}$. Our analysis of the alignment due to the motion (4.2) will use an observation due to Szeri [73]: the non-linear equation (4.2) can be solved by considering a companion linear equation for a vector $\boldsymbol{x}(t)$, which evolves under the action of a time-dependent matrix $\mathbf{M}(t)$:

$$\boldsymbol{x}(t) = \mathbf{M}(t)\boldsymbol{x}(0) \,, \quad \frac{\mathrm{d}\mathbf{M}}{\mathrm{d}t} = \mathbf{A}(t)\,\mathbf{M} \tag{4.4}$$

where the initial conditions are $\mathbf{M}(0) = \mathbf{I}$ (the identity matrix) and $\boldsymbol{x}(0) = \mathbf{n}(0)$. The solution to (4.2) is obtained by normalising the solution of (4.4):

$$\mathbf{n}(t) = \frac{\boldsymbol{x}(t)}{|\boldsymbol{x}(t)|} \,. \tag{4.5}$$

The advantage of this approach is that it is easier to solve the linear equation (4.4) than the non-linear equation (4.2).

4.2.2 Ornstein-Uhlenbeck model for velocity gradients in isotropic flows

In this section we describe a simple stochastic model for the matrix $\mathbf{A}(t)$ in isotropic random flows. A version of this model was used by Vincenzi *et al* [74], and its structure is suggested by the observations in [71]. The model was also considered in [69], which gave a detailed account of its implementation. It is known that the elements of $\mathbf{S}$ and $\mathbf{\Omega}$ fluctuate randomly about zero, with different timescales τ_s and τ_v respectively. Their correlation functions are well approximated by exponential functions. This suggests modelling the elements of $\mathbf{S}$ and $\mathbf{\Omega}$ by Ornstein-Uhlenbeck processes [75, 25]. The three independent components of the vorticity will be modelled by:

$$\dot{\Omega}_{ij} = -\frac{1}{\tau_\mathrm{v}}\Omega_{ij} + \sqrt{2\,D_\mathrm{v}}\eta_{ij}(t) \tag{4.6}$$

where D_v is the diffusion constant associated with vorticity and $\eta_{ij}(t)$ are independent white-noise signals, satisfying

$$\langle \eta(t) \rangle = 0 \ , \quad \langle \eta(t)\eta(t') \rangle = \delta(t-t') \ . \tag{4.7}$$

This model predicts that the correlation function of Ω_{ij} is exponential [75, 25]:

$$\langle \Omega_{ij}(t_1)\Omega_{ij}(t_2) \rangle = D_\mathrm{v}\tau_\mathrm{v} \exp(-|t_1 - t_2|/\tau_\mathrm{v}) \ . \tag{4.8}$$

The components of the strain-rate matrix are generated by a further six Ornstein-Uhlenbeck processes, with a different correlation time τ_s. The off-diagonal elements are generated by a process of the same form as (4.6), with the diffusion coefficient in (4.7) replaced by D_s. The diagonal elements of the strain-rate matrix must satisfy $\sum_{i=1}^{3} S_{ii} = 0$, which is the incompressibility condition, $\boldsymbol{\nabla} \cdot \boldsymbol{u} = 0$. This constraint is satisfied by the solution of the following Ornstein-Uhlenbeck equations (see 1.3.2)

$$\dot{S}_{ii} = -\frac{1}{\tau_\mathrm{s}}S_{ii} + \sqrt{2\,D_\mathrm{d}}\left[\eta_{ii}(t) - \frac{1}{3}\sum_{j=1}^{3}\eta_{jj}(t)\right] \ . \tag{4.9}$$

The elements Ω_{ij} and S_{ij} generated by these processes are statistically independent, apart from the constraint that $\sum_i S_{ii} = 0$. The variances of the off-diagonal, diagonal and vorticity elements are respectively denoted $\langle S_\mathrm{o}^2 \rangle$, $\langle S_\mathrm{d}^2 \rangle$ and $\langle \Omega^2 \rangle$, and are related to the relaxation times and diffusion rates by $\langle S_\mathrm{o}^2 \rangle = D_\mathrm{s}\tau_\mathrm{s}$, $\langle S_\mathrm{d}^2 \rangle = \frac{2}{3}D_\mathrm{d}\tau_\mathrm{s}$ and $\langle \Omega^2 \rangle = D_\mathrm{v}\tau_\mathrm{v}$. The requirement that the statistics of the model are invariant under rotations (so that it describes a velocity gradient with isotropic statistics) gives $D_\mathrm{d} = 2D_\mathrm{s}$, so that this model has four parameters: τ_s, τ_v, D_s and D_v. Note that the diffusion coefficients have dimension $[D] = T^{-3}$, implying that the model has three independent dimensionless parameters. In the following we consider the limit as $\tau_\mathrm{v}/\tau_\mathrm{s} \to \infty$, so that the vorticity is frozen, with angular velocity ω. We also assume that $D_\mathrm{s}\tau_\mathrm{s}^3 \ll 1$, so that the strain fluctuations are small. This leaves one dimensionless parameter, which we will take to be $\zeta = \omega\tau_\mathrm{s}$.

4.3 Transformation to an axisymmetric pure strain model

4.3.1 The frozen vorticity limit

In this section we consider the alignment of rod-like particles in an isotropic flow, where there is a non-zero vorticity which is slowly varying. The approach is to transform the equation of motion to a reference frame which rotates around the axis of vorticity. In this coordinate system, the strain field oscillates in directions which are perpendicular to the vorticity vector, in addition to having random temporal fluctuations. The effect of these oscillations is to reduce the effective intensity of the random strain field in directions perpendicular to the vorticity vector, so that an isotropic problem with vorticity is transformed to an axisymmetric model with a velocity gradient which is a pure strain. This reduction was also discussed in [69]. In order to isolate the effect of the vorticity in the equation of motion for the time dependent matrix, $\mathbf{M}$, we introduce another time dependent matrix $\mathbf{M}_0$ which evolves under the vorticity alone:

$$\dot{\mathbf{M}} = (\mathbf{S} + \boldsymbol{\Omega})\mathbf{M} \ , \quad \dot{\mathbf{M}}_0 = \boldsymbol{\Omega}\,\mathbf{M}_0 \ . \tag{4.10}$$

Note that $\mathbf{M}_0(t)$ is just a rotation matrix, describing rotation about an axis in the direction of the vorticity vector $\boldsymbol{\omega}$. The two time dependent matrices may be related by writing

$$\mathbf{M}(t) = \mathbf{M}_0(t)\mathbf{K}(t) \tag{4.11}$$

where $\mathbf{K}(t)$ is an evolution matrix which describes the effect of the shear. An elementary calculation shows that $\mathbf{K}$ has the equation of motion

$$\dot{\mathbf{K}} = \boldsymbol{\sigma}(t)\mathbf{K} \tag{4.12}$$

where

$$\boldsymbol{\sigma} = \mathbf{M}_0^{-1}\mathbf{S}\mathbf{M}_0 \tag{4.13}$$

is obtained from $\mathbf{S}$ by applying a time-dependent rotation. Consider the form of the matrix $\boldsymbol{\sigma}$. In the case where the vorticity vector is frozen, and equal to $\boldsymbol{\Omega}_0$, the matrix $\mathbf{M}_0$ is a rotation matrix: $\mathbf{M}_0 = \exp(\boldsymbol{\Omega}_0\, t)$. Without loss of generality we can consider the case where the vorticity is aligned with the z-axis, with magnitude $\Omega = 2\omega$, where ω is the rotational angular velocity, so that $\mathbf{M}_0$ is a rotation matrix of the form

$$\mathbf{M}_0 = \exp(\boldsymbol{\Omega}_0 t) = \mathbf{R}(\omega t) = \begin{pmatrix} \cos\omega t & -\sin\omega t & 0 \\ \sin\omega t & \cos\omega t & 0 \\ 0 & 0 & 1 \end{pmatrix} \equiv \begin{pmatrix} c & -s & 0 \\ s & c & 0 \\ 0 & 0 & 1 \end{pmatrix} . \tag{4.14}$$

If the elements of $\mathbf{S}$ are S_{ij}, the elements of $\boldsymbol{\sigma}$ are

$$\boldsymbol{\sigma} = \begin{pmatrix} c^2S_{11} + s^2S_{22} + 2csS_{12} & (c^2 - s^2)S_{12} + cs(S_{22} - S_{11}) & cS_{13} - sS_{23} \\ (c^2 - s^2)S_{12} + cs(S_{22} - S_{11}) & s^2S_{11} + c^2S_{22} - 2csS_{12} & cS_{23} + sS_{13} \\ cS_{13} - sS_{23} & cS_{23} + sS_{13} & S_{33} \end{pmatrix} .$$

Note that all of the off-diagonal components oscillate with angular frequency ω or 2ω. The diagonal component in the direction of the vorticity vector does not oscillate, but the other diagonal elements contain both oscillatory terms and non-oscillatory terms.

4.3.2 Limit of short correlation time for strain rate

Now consider the case where the strain rate $\mathbf{S}$ is sufficiently small that the strain which accumulates over its correlation time τ_s is very small. In this case the evolution of the matrix $\mathbf{K}$ (defined by equation (4.12)) can be described by a diffusive process. Specifically, we consider the evolution of (4.12) over a time period δt which is large compared to the correlation time of the strain field τ_s, but still sufficiently small that the strain which accumulates over this time interval is small. We write

$$\mathbf{K}(t + \delta t) = (\mathbf{I} + \delta\boldsymbol{\Sigma}(\delta t, t))\ \mathbf{K}(t) \tag{4.15}$$

where the $\delta\boldsymbol{\Sigma}$ are small and may be assumed to be random matrices, chosen independently at each timestep. We characterise the evolution (4.12) by computing the statistics of the random strain increments $\delta\boldsymbol{\Sigma}$, which are in turn obtained from the random strain $\mathbf{S}(t)$ using (4.12) and (4.14). The advantage of considering the small elements $\boldsymbol{\Sigma}$ is that they are small random increments which are applied independently at each timestep. This enables their effect to be analysed using a Fokker-Planck equation. First consider the relation between the elements of the matrices $\delta\boldsymbol{\Sigma}$ and $\boldsymbol{\sigma}$. By integrating (4.12) and using the definition (4.15) we obtain

$$\delta\boldsymbol{\Sigma}(\delta t, t) = \int_t^{t+\delta t} \mathrm{d}t'\ \boldsymbol{\sigma}(t')\ (\mathbf{I} + \delta\boldsymbol{\Sigma}(t' - t, t))\ . \tag{4.16}$$

Iterating this expression, taking $t = 0$, and suppressing the initial time t in the arguments of $\delta\boldsymbol{\Sigma}$ we obtain

$$\delta\boldsymbol{\Sigma}(\delta t) = \int_0^{\delta t} \mathrm{d}t_1\ \boldsymbol{\sigma}(t_1) + \int_0^{\delta t} \mathrm{d}t_1 \int_0^{t_1} \mathrm{d}t_2\ \boldsymbol{\sigma}(t_1)\boldsymbol{\sigma}(t_2) + O(\sigma^3)\ . \tag{4.17}$$

Using the fact that the correlation time is assumed to satisfy $\delta t \gg \tau_s$, we can write

$$\delta\boldsymbol{\Sigma}(\delta t) = \int_0^{\delta t} \mathrm{d}t\ \boldsymbol{\sigma}(t) + \frac{\delta t}{2} \int_{-\infty}^{\infty} \mathrm{d}t\ \langle\boldsymbol{\sigma}(t)\boldsymbol{\sigma}(0)\rangle + O(\delta t^{3/2})\ . \tag{4.18}$$

The first of term is a random variable with mean zero and size $O(\delta t^{1/2})$, giving rise to a diffusion term in a Fokker-Planck equation. The second term represents a drift at a velocity which is well-defined in

the limit as $\delta t \to 0$. The remaining terms may be neglected. In order to formulate the Fokker-Planck equation, we must determine the statistics of the increments $\delta\Sigma_{ij}(\delta t)$.

If $\omega\tau_{\rm s} \ll 1$, the effect of the oscillatory terms in equation (4.14) is negligible. Let us consider how to treat the problem when $\omega\tau_{\rm s}$ is not small. To simplify the discussion, consider the quantity

$$\delta F = \int_0^{\delta t} {\rm d}t \; f(t)\cos(\omega t) \tag{4.19}$$

where $\delta t/\tau_{\rm s} \gg 1$, and where $f(t)$ is a random function which satisfies

$$\langle f(t)\rangle = 0 \; , \quad \langle f(t)f(t')\rangle = C(t-t') \; . \tag{4.20}$$

The spectral intensity $I(\nu)$ of the fluctuations of $f(t)$ is defined by

$$I(\nu) = \int_{-\infty}^{\infty} {\rm d}t \; \exp({\rm i}\nu t)\, C(t) \tag{4.21}$$

and we shall assume that $C(-t) = C(t)$, so that $I(-\omega) = I(\omega)$. The expectation value of δF is equal to zero. Its variance is

$$\begin{aligned}
\langle \delta F^2\rangle &= \int_0^{\delta t} {\rm d}t_1 \int_0^{\delta t} {\rm d}t_2 \; \langle f(t_1)f(t_2)\rangle \cos(\omega t_1)\cos(\omega t_2) \\
&= \frac{1}{2}\int_0^{\delta t} {\rm d}t_1 \int_0^{\delta t} {\rm d}t_2 \; C(t_1-t_2)[\cos(\omega(t_1-t_2)) + \cos(\omega(t_1+t_2))] \\
&= \frac{1}{2}\delta t \int_{-\infty}^{\infty} {\rm d}s \; C(s)\cos(\omega s) + O(\delta t^2) \\
&= \frac{1}{4}\delta t[I(\omega) + I(-\omega)] + O(\delta t^2) = \frac{1}{2}\delta t\, I(\omega) + O(\delta t^2) \; .
\end{aligned} \tag{4.22}$$

The third steps assumes that $\omega\delta t \gg 1$, as well as $\delta t/\tau \gg 1$. Now consider the effect of the random strain model defined by (4.7)-(4.9) in the limit where the timescale $\tau_{\rm s}$ of the fluctuations of $S_{ij}(t)$ is very small. We assume that the functional form of the spectral intensity of each component S_{ij} is the same, but that their variances are different, so that the spectral intensity of $S_{ij}(t)$ is $\langle S_{ij}^2\rangle I(\nu)$, implying that the intensity function is normalised so that $I(0) = 1$. We represent the effect of the randomly fluctuating strain field described by (4.14) by an effective strain field with diffusive fluctuations. Note that δt is assumed to satisfy $\delta t/\tau \gg 1$, despite being 'small '. By applying (4.22),

variance of $\delta\Sigma_{11}$ is

$$
\begin{aligned}
&\langle \delta\Sigma_{11}^2 \rangle \\
&= \int_0^{\delta t} \mathrm{d}t_1 \int_0^{\delta t} \mathrm{d}t_2 \left\langle \left[\frac{1}{2}(1+\cos 2\omega t_1) S_{11}(t_1) + \frac{1}{2}(1-\cos 2\omega t_2) S_{22}(t_1) + \sin 2\omega t_1 S_{12}(t_1) \right] \right. \\
&\quad \left. \times \left[\frac{1}{2}(1+\cos 2\omega t_2) S_{11}(t_2) + \frac{1}{2}(1-\cos 2\omega t_2) S_{22}(t_2) + \sin 2\omega t_2 S_{12}(t_2) \right] \right\rangle \\
&= \delta t \int_{-\infty}^{\infty} \mathrm{d}\tau \, \frac{1}{8}[2+\cos 2\omega\tau] \, \langle S_{11}(\tau) S_{11}(0) \rangle + \frac{1}{8}[2+\cos 2\omega\tau] \, \langle S_{22}(\tau) S_{22}(0) \rangle \\
&\quad + \frac{1}{2}\cos(2\omega\tau) \, \langle S_{12}(\tau) S_{12}(0) \rangle + \frac{1}{4}[2-\cos(2\omega\tau)] \langle S_{11}(\tau) S_{22}(0) \rangle + O(\delta t^2) \\
&= \frac{\delta t}{8}[2+I(2\omega)] \langle S_{11}^2 \rangle + \frac{\delta t}{8}[2+I(2\omega)] \langle S_{22}^2 \rangle + \frac{\delta t}{2} I(2\omega) \langle S_{12}^2 \rangle \\
&\quad + \frac{\delta t}{4}[2-I(2\omega)] \langle S_{11} S_{22} \rangle \; + O(\delta t^2)
\end{aligned}
\tag{4.23}
$$

Using the same approach, the full set of non-zero covariances of $\delta\Sigma_{ij}$ is

$$
\begin{aligned}
\langle \delta\Sigma_{11}^2 \rangle = \langle \delta\Sigma_{22}^2 \rangle &= \frac{\delta t}{4} \left[(2+I(2\omega)) \langle S_{11}^2 \rangle + (2-I(2\omega)) \langle S_{11} S_{22} \rangle + 2I(2\omega) \langle S_{12}^2 \rangle \right] \\
\langle \delta\Sigma_{11} \delta\Sigma_{22} \rangle &= \frac{\delta t}{4} \left[(2-I(2\omega)) \langle S_{11}^2 \rangle + (2+I(2\omega)) \langle S_{11} S_{22} \rangle - 2I(2\omega) \langle S_{12}^2 \rangle \right] \\
\langle \delta\Sigma_{12}^2 \rangle &= \frac{\delta t}{4} \left[I(2\omega) \langle S_{11}^2 \rangle - I(2\omega) \langle S_{11} S_{22} \rangle + 2I(2\omega) \langle S_{12}^2 \rangle \right] \\
\langle \delta\Sigma_{33}^2 \rangle &= \delta t \, I(0) \, \left[\langle 2S_{11}^2 \rangle + 2\langle S_{11} S_{22} \rangle \right] \\
\langle \Sigma_{13}^2 \rangle = \langle \Sigma_{23}^2 \rangle &= \delta t I(\omega) \langle S_{13}^2 \rangle \; .
\end{aligned}
\tag{4.24}
$$

Finally, we must consider the mean values of the increments $\delta\Sigma_{ij}(\delta t)$. As an example, consider the evaluation of $\langle \delta\Sigma_{11} \rangle$. From the second term in the right hand side of (4.18), we have

$$
\begin{aligned}
\langle \delta\Sigma_{11} \rangle &= \frac{\delta t}{2} \int_{-\infty}^{\infty} \mathrm{d}t \, \sum_{j=1}^{3} \langle \sigma_{1j}(t) \sigma_{j1}(0) \rangle \\
&= \frac{\delta t}{2} \int_{-\infty}^{\infty} \mathrm{d}t \; c^2 \langle S_{11}(t) S_{11}(0) \rangle + s^2 \langle S_{11}(t) S_{22}(0) \rangle \\
&\quad + (c^2 - s^2) \langle S_{12}(t) S_{12}(0) \rangle + c \langle S_{13}(t) S_{13}(0) \rangle \\
&= \frac{\delta t}{4} \left[(1+I(2\omega)) \langle S_{11}^2 \rangle + (I-I(2\omega)) \langle S_{11} S_{22} \rangle + 2I(2\omega) \langle S_{12}^2 \rangle + 2I(\omega) \langle S_{13}^2 \rangle \right] \; .
\end{aligned}
\tag{4.25}
$$

Only the diagonal elements of $\delta\boldsymbol{\Sigma}$ have a non-zero contribution to the mean at $O(\delta t)$: we define

velocity coefficients μ_j as follows

$$\begin{aligned}
\langle \delta\Sigma_{11} \rangle &= \mu_1 \delta t = \frac{\delta t}{4}\Big[(1+I(2\omega))\langle S_{11}^2\rangle + (I-I(2\omega))\langle S_{11}S_{22}\rangle \\
&\qquad + 2I(2\omega)\langle S_{12}^2\rangle + 2I(\omega)\langle S_{13}^2\rangle\Big] \\
\langle \delta\Sigma_{22} \rangle &= \mu_2 \delta t = \mu_1 \delta t \\
\langle \delta\Sigma_{33} \rangle &= \mu_3 \delta t = \frac{\delta t}{4}\left[4\langle S_{11}^2\rangle + 4\langle S_{11}S_{22}\rangle + 4I(\omega)\langle S_{13}^2\rangle\right] .
\end{aligned} \tag{4.26}$$

4.3.3 Uniaxial random strain in three dimensions

In sections 4.3.1 and 4.3.2 we showed how an isotropic model with frozen vorticity and rapidly fluctuating strain can be represented by an axisymmetric model where the velocity gradient is a pure strain $\boldsymbol{\sigma}$. In the limit where the strain which occurs over the correlation time τ_s is small, the effect of this strain is represented by a product of matrices $\mathbf{I}+\delta\boldsymbol{\Sigma}$, where the small increments $\delta\boldsymbol{\Sigma}$ are independently distributed at each timestep of size δt. They have diffusive fluctuations, so that $\delta\boldsymbol{\Sigma} = O(\delta t^{1/2})$. The matrix $\boldsymbol{\sigma}$ is traceless, representing the fact that the velocity field is incompressible. The matrix $\delta\boldsymbol{\Sigma}$ need not, however, satisfy $\mathrm{tr}(\delta\boldsymbol{\Sigma}) = 0$, although it is clear that the leading order term in (4.18) is traceless. In this section we discuss how to parametrise such axisymmetric strain fields.

We take this axis of rotational symmetry to be $\mathbf{e}_3$; the general case is obtained from this one by applying rotation matrices. The strain is described by a 3×3 matrix $\delta\boldsymbol{\Sigma}$, which we write in the form

$$\delta\boldsymbol{\Sigma} = \begin{pmatrix} \delta A & \delta C & \delta D \\ \delta C & \delta B & \delta E \\ \delta D & \delta E & -(\delta A+\delta B) \end{pmatrix} + \begin{pmatrix} \mu_1\delta t & 0 & 0 \\ 0 & \mu_1\delta t & 0 \\ 0 & 0 & \mu_3\delta t \end{pmatrix} \tag{4.27}$$

where δA, δB, δC, δD and δE are random variables with mean value zero, and diffusive fluctuations: $\langle \delta A\rangle = 0$ and $\langle \delta A^2\rangle = 2D_{AA}\delta t$, $\langle \delta A\delta B\rangle = 2D_{AB}\delta t$, etc. Applying a rotation about the $\mathbf{e}_3$ axis by angle θ to the random component of $\delta\boldsymbol{\Sigma}$ gives a transformed matrix, with elements $\delta A'$, $\delta B'$, $\delta C'$, $\delta D'$ and $\delta E'$, given by

$$\begin{aligned}
\delta A' &= \cos^2\theta\delta A + \sin^2\theta\delta B + 2\cos\theta\sin\theta\delta C \\
\delta B' &= \sin^2\theta\delta A + \cos^2\theta\delta B - 2\cos\theta\sin\theta\delta C \\
\delta C' &= (\cos^2\theta - \sin^2\theta)\delta C + \cos\theta\sin\theta(\delta B - \delta A) \\
\delta D' &= \cos\theta\delta D + \sin\theta\delta E \\
\delta E' &= \cos\theta\delta E - \sin\theta\delta D
\end{aligned} \tag{4.28}$$

where $c = \cos\theta$ and $s = \sin\theta$. The non-random diagonal component is invariant under rotation about $\mathbf{e}_3$. Note that $\delta A' + \delta B' = \delta A + \delta B$, so that the element $\delta\Sigma_{33}$ is invariant under rotation.

We require that the statistics of the elements are invariant under the rotation angle θ. It is clear that δA and δB must have the same variance, as must δD and δE. Without loss of generality, we can consider a model with $\langle \delta A^2 \rangle = 2\delta t$. We therefore characterise the model by the following statistics, where α, β, γ are three constants:

$$\begin{aligned} \langle \delta A^2 \rangle = \langle \delta B^2 \rangle &= 2\delta t \\ \langle \delta A \delta B \rangle &= 2\alpha\delta t \\ \langle \delta C^2 \rangle &= 2\beta\delta t \\ \langle \delta D^2 \rangle = \langle \delta E^2 \rangle &= 2\gamma\delta t \ . \end{aligned} \tag{4.29}$$

Other covariances, such as $\langle \delta B \delta E \rangle$, are equal to zero. The requirement that the statistics of the rotated matrix are independent of θ leads to the equations

$$\begin{aligned} \langle \delta A'^2 \rangle &= 2[c^4 + s^4 + 2c^2 s^2 \alpha + 4c^2 s^2 \beta]\delta t = 2\delta t \\ \langle A'B' \rangle &= 2[-4c^2 s^2 \beta + 2c^2 s^2 + (c^4 + s^4)\alpha]\delta t = 2\alpha\delta t \\ \langle C'^2 \rangle &= 2[(c^4 + s^4 - 2c^2 s^2)\beta + c^2 s^2 (2 - 2\alpha)]\delta t = 2\beta\delta t \ . \end{aligned} \tag{4.30}$$

Rotational invariance therefore leads to an equation which must the satisfied by α and β:

$$\alpha + 2\beta = 1 \tag{4.31}$$

so that the model for a uniaxial random strain has four independent parameters, which we can take to be α, γ, μ_1 and μ_3.

For a special choice of these parameters the model is isotropic. Clearly this requires $\mu_1 = \mu_3$. Also, requiring $\langle \delta C^2 \rangle = \langle \delta D^2 \rangle = \langle \delta E^2 \rangle$ gives $\gamma = \beta$. Also, requiring $\langle (\delta A + \delta B)^2 \rangle = \langle \delta A^2 \rangle = \langle \delta B^2 \rangle$ gives $2 + 2\alpha = 1$. Solving these equations we find that the the covariances of the random terms are fixed in the isotropic case

$$\alpha = -\frac{1}{2} \ , \quad \beta = \gamma = \frac{3}{4} \ , \quad \mu_3 = \mu_1 \ . \tag{4.32}$$

Another notable limit of the model is the case where the matrix is diagonal: this model is $\beta = \gamma = 0$, implying $\alpha = 1$.

4.4 Alignment in random strain fields

4.4.1 General solution in a diffusive axisymmetric strain

In section 4.3 we described the construction of a model for the alignment of microscopic rods with vorticity, in which the velocity gradient is represented as a strain field with diffusive fluctuations, axisymmetric about the direction of the vorticity. First we consider the alignment of rod-like particles under a succession of independent random shears $\mathbf{I}+\delta\mathbf{\Sigma}$, which satisfy the conditions derived in section 4.3.3 for the shear statistics to be uniaxial, before discussing the specific model for rod alignment in section 4.2. Using the approach summarised by equations (4.4) and (4.5), the direction vector $\mathbf{n}$ of a rod-like particle evolves according to the linear equation

$$(\mathbf{I}+\delta\mathbf{\Sigma})\mathbf{n}(t) = (1+\delta R)\mathbf{n}(t+\delta t) \tag{4.33}$$

where $\delta\mathbf{\Sigma}$ is the infinitesimal strain in time δt, previously introduced in equation (4.16), and δR is the fractional change in length of the vector under the linear evolution equation. Write $\mathbf{n}(t+\delta t) = \mathbf{n}(t) + \delta\mathbf{n} + O(\delta\mathbf{n}^2)$, where $\delta\mathbf{n}\cdot\mathbf{n} = 0$. Because of rotational symmetry about the z-axis, we can assume without loss of generality that the y component of $\mathbf{n}$ is equal to zero. We therefore consider the following orthogonal basis of unit vectors

$$\begin{aligned}\mathbf{n} &= (\sin\theta, 0, \cos\theta) = (x, 0, z)\\ \mathbf{m} &= (-\cos\theta, 0, \sin\theta) = (-z, 0, x)\\ \mathbf{k} &= (0, 1, 0)\ .\end{aligned} \tag{4.34}$$

where θ is the polar angle, and $z = \cos\theta$. Writing $\delta\mathbf{n} = \delta X\mathbf{m} + \delta Y\mathbf{k}$, we have

$$\mathbf{n}(t+\delta t) = \mathbf{n} + \delta X\mathbf{m} + \delta Y\mathbf{k} - \frac{1}{2}(\delta X^2 + \delta Y^2)\mathbf{n} + O(\delta\mathbf{n}^3)\ . \tag{4.35}$$

By taking the dot product of (4.33) in turn with $\mathbf{n}$, $\mathbf{m}$ and $\mathbf{k}$, we find, respectively to leading order

$$\delta R \sim \mathbf{n}\cdot\delta\mathbf{\Sigma}\,\mathbf{n} \equiv \delta\Sigma_{nn} \tag{4.36}$$

and

$$\begin{aligned}\mathbf{m}\cdot\delta\mathbf{n}(1+\delta R) &\sim \mathbf{m}\cdot\delta\mathbf{\Sigma}\,\mathbf{n} \equiv \delta\Sigma_{mn}\\ \mathbf{k}\cdot\delta\mathbf{n}(1+\delta R) &\sim \mathbf{k}\cdot\delta\mathbf{\Sigma}\,\mathbf{n} \equiv \delta\Sigma_{kn}\end{aligned} \tag{4.37}$$

Let us characterise the evolution of $\mathbf{n}$ through the evolution of its projection onto the $\mathbf{e}_3$ axis, namely

$$z = \mathbf{e}_3 \cdot \mathbf{n} \ . \tag{4.38}$$

This is a convenient choice because z will have a uniform probability density function for an isotropic strain field. Using (4.35), we find that

$$z + \delta z \equiv \mathbf{e}_3 \cdot \mathbf{n}(t + \delta t) = \cos\theta + \sin\theta \delta X - \frac{1}{2}\cos\theta(\delta X^2 + \delta Y^2) \ . \tag{4.39}$$

We define the drift velocity v_z and diffusion coefficient D_z of z by

$$\langle \delta z \rangle = v_z \delta t \ , \quad \langle \delta z^2 \rangle = 2 D_z \delta t \ . \tag{4.40}$$

Using (4.41) and (4.36), (4.37) we obtain

$$v_z \delta t = x\langle \delta\Sigma_{mn} - \delta\Sigma_{nn}\delta\Sigma_{mn} \rangle - \frac{z}{2}\langle \delta S_{mn}^2 + \delta\Sigma_{kn}^2 \rangle + O(\delta t^{3/2}) \tag{4.41}$$

and

$$D_z \delta t = \frac{1}{2}(1 - z^2)\langle \delta\Sigma_{mn}^2 \rangle + O(\delta t^{3/2}) \ . \tag{4.42}$$

Now consider that statistics of the fluctuations of z for the uniaxial strain model. For the model defined in section 4.3.3, we have

$$\begin{aligned}
\delta\Sigma_{nn} &= \delta A x^2 + 2\delta D xz - (\delta A + \delta B)z^2 + \mu_1 x^2 \delta t + \mu_3 z^2 \delta t \\
\delta\Sigma_{mn} &= \delta D(x^2 - z^2) - (2\delta A + \delta B)xz + (\mu_3 - \mu_1)xz\delta t \\
\delta\Sigma_{kn} &= \delta C x + \delta E z
\end{aligned} \tag{4.43}$$

where $x = \sqrt{1 - z^2}$. We can combine these relations with (4.41) and (4.42) to determine D_z and v_z:

$$\begin{aligned}
D_z \delta t &= \frac{1 - z^2}{2}\langle [\delta D(1 - 2z^2) - (2\delta A + \delta B)xz]^2 \rangle \\
v_z \delta t &= -x\langle [\delta A(1 - 2z^2) - \delta B z^2 + 2\delta D xz][\delta D(1 - 2z^2) - (2\delta A + \delta B)xz] \rangle \\
&\quad - \frac{z}{2}\langle [\delta D(1 - 2z^2) - (2\delta A + \delta B)xz]^2 \rangle - \frac{z}{2}\langle [\delta C x + \delta E z]^2 \rangle + \Delta\mu x^2 z \delta t
\end{aligned} \tag{4.44}$$

where $\Delta\mu = \mu_3 - \mu_1$. At this point MAPLE was used to keep track of the calculation, and solve the resultant equation. Using the statistics of the elements δA, δB, δC, δD and δE, and ordering the

resulting expressions as polynomials in z we obtain:

$$\begin{aligned} D_z &= \frac{1}{2}(1-x^2)\left[\gamma + (5+4\alpha-4\gamma)z^2 - (5+4\alpha-4\gamma)z^4\right] \\ v_z &= \left(\frac{7}{4}+\frac{5}{4}\alpha-\frac{5}{2}\gamma+\Delta\mu\right)z + \left(-\frac{37}{4}-\frac{29}{4}\alpha+\frac{15}{2}\gamma-\Delta\mu\right)z^3 \\ &\quad + \left(\frac{15}{2}+6\alpha-6\gamma\right)z^5 \,. \end{aligned} \tag{4.45}$$

The steady-state probability density for z, namely $P(z)$, satisfies

$$v_z(z)P(z) = \frac{\mathrm{d}}{\mathrm{d}z}\left(D_z(z)P(z)\right) \,. \tag{4.46}$$

In the isotropic case, we have $\alpha = -1/2$ and $\gamma = 3/4$. In this case we find

$$D_z = \frac{3}{8}(1-z^2) \,, \quad v_z = -\frac{3}{4}z \,, \quad \text{(isotropic case)} \tag{4.47}$$

and the normalised solution is $P(z) = \frac{1}{2}$ for $-1 \le z \le 1$. In the general case, we find that $(1-z^2)$ is a factor of $v_z - D_z'$, and the differential equation (4.46) is

$$\frac{1}{P}\frac{\mathrm{d}P}{\mathrm{d}z} = \frac{-z\left[6(5+4\alpha-4\gamma)z^2 - 13 - 11\alpha + 10\gamma + 4\Delta\mu\right]}{4\left[\gamma + (5+4\alpha-4\gamma)z^2 - (5+4\alpha-4\gamma)z^4\right]} \tag{4.48}$$

it us useful to change the variable to $u = z^2$. In terms of u, the differential equation (4.48) may be written

$$\frac{1}{P}\frac{\mathrm{d}P}{\mathrm{d}u} = -\frac{6(5+4\alpha-4\gamma)u - 13 - 11\alpha + 10\gamma + 4\Delta\mu}{8\left[\gamma + (5+4\alpha-4\gamma)u - (5+4\alpha-4\gamma)u^2\right]} \,. \tag{4.49}$$

Representing the right-hand-side using partial fractions, we obtain

$$\frac{1}{P}\frac{\mathrm{d}P}{\mathrm{d}u} = \frac{c_+}{u_+ - u} + \frac{c_-}{u - u_-} \tag{4.50}$$

where $u_\pm$ are the roots of the denominator on the right-hand-side of (4.49)

$$u_\pm = \frac{1}{2} \pm \frac{1}{2}\sqrt{1 + \frac{4\gamma}{5+4\alpha-4\gamma}} \tag{4.51}$$

and where the coefficients are

$$c_\pm = \frac{(4\Delta\mu - 2\alpha + \gamma - 2)u_\pm - 13 - 11\alpha - 2\gamma - 4\Delta\mu}{4(5+4\alpha)} \,. \tag{4.52}$$

The probability density expressed in terms of z is then

$$P(z) = \mathcal{C}\,(z^2 - u_-)^{c_-}(z^2 - u_+)^{c_+} \tag{4.53}$$

where C is a normalisation constant.

4.4.2 Solution of rod alignment model

Now we apply the solution obtained in section 4.1 to the model for alignment of microscopic rods, as developed in sections 2 and 3. In section 2.2 we introduced the Ornstein-Uhlenbeck model for a random, isotropic velocity gradient field. The theory in section 3 made two assumptions. In section 3 it was assumed that the vorticity varies slowly, and section 3.1 made a further assumption that the strain field is small. Let us consider the implications of these assumptions for the parameters of the model. The assumption that the vorticity varies slowly implies that τ_v is large compared to other timescales in the system of equations. The typical strain rate $|S| = \sqrt{\langle \mathrm{tr}(\mathbf{S}^2)\rangle}$ and the correlation time τ_s should satisfy $|S|\tau_s \ll 1$. The solution of the Ornstein-Uhlenbeck process implies

$$\langle \mathrm{tr}(\mathbf{S}^2)\rangle = 10 D_s \tau_s \tag{4.54}$$

so that the criterion for the strain to be small is simply $D_s\tau_s^3 \ll 1$. The angular velocity ω is related to the magnitude of the vorticity Ω by $\Omega = 2\omega$. The magnitude of the vorticity is estimated by $\langle \Omega^2\rangle = \mathrm{tr}\langle(\mathbf{\Omega}^2)\rangle = 3D_v\tau_v$. The rotation rate ω has a Gaussian distribution, with variance

$$\sigma^2 = \langle \omega^2\rangle = \frac{3}{4} D_v \tau_v \, . \tag{4.55}$$

Because the Ornstein-Uhlenbeck model has an exponential decay of correlations, given by equation (4.8), spectral intensity of the strain fluctuations is a Lorentzian function:

$$I(\nu) = \frac{1}{1+\nu^2\tau_s^2} \, . \tag{4.56}$$

In order to apply the results in section 4.1 we must specify the covariances of the fluctuations of the axisymmetric effective strain tensor. If we normalise the variances so that $\langle S_{11}^2\rangle = 1$, $\langle S_{11}S_{22}\rangle = \alpha$,

$\langle S_{12}^2\rangle = \beta$, $\langle S_{13}^2\rangle = \gamma$, the non-zero covariances and expectation values of $\delta\Sigma_{ij}$ are

$$\begin{aligned}
\langle \delta\Sigma_{11}^2\rangle = \langle \delta\Sigma_{22}^2\rangle &= \delta t\left[I(0)\left(\frac{1}{2}+\frac{\alpha}{2}\right)+I(2\omega)\left(\frac{1}{4}-\frac{\alpha}{4}+\frac{\beta}{2}\right)\right]\\
\langle \delta\Sigma_{11}\delta\Sigma_{22}\rangle &= \delta t\left[I(0)\left(\frac{1}{2}+\frac{\alpha}{2}\right)-I(2\omega)\left(\frac{1}{4}-\frac{\alpha}{4}+\frac{\beta}{2}\right)\right]\\
\langle \delta\Sigma_{12}^2\rangle &= \delta t\left[I(2\omega)\left(\frac{1}{4}-\frac{\alpha}{4}+\frac{\beta}{2}\right)\right]\\
\langle \Sigma_{13}^2\rangle = \langle \Sigma_{23}^2\rangle &= \delta t I(\omega)\gamma\\
\langle \delta\Sigma_{33}^2\rangle &= 2\,\delta t\, I(0)\,(1+\alpha)\\
\langle \delta\Sigma_{11}\rangle = \langle \delta\Sigma_{22}\rangle &= \delta t\left[I(0)\left(\frac{1}{4}+\frac{\alpha}{4}\right)+I(\omega)\frac{\gamma}{2}+I(2\omega)\left(\frac{1}{4}-\frac{\alpha}{4}+\frac{\beta}{2}\right)\right]\\
\langle \delta\Sigma_{33}\rangle &= \delta t\,[I(0)(1+\alpha)+I(\omega)\gamma]\ .
\end{aligned} \tag{4.57}$$

We use the assumption that the original random strain field S_{ij} is isotropic, so that the statistics of these elements satisfy (4.32). Using (4.57) we obtain

$$\begin{aligned}
\langle \delta\Sigma_{11}^2\rangle = \langle \delta\Sigma_{22}^2\rangle &= \frac{\delta t}{4}[1+3I(2\omega)]\\
\langle \delta\Sigma_{11}\delta\Sigma_{22}\rangle &= \frac{\delta t}{4}[1-3I(2\omega)]\\
\langle \delta\Sigma_{12}^2\rangle &= \frac{\delta t}{4}3I(2\omega)\\
\langle \delta\Sigma_{13}^2\rangle = \langle \delta\Sigma_{23}^2\rangle &= \frac{\delta t}{4}3I(\omega)\\
\langle \delta\Sigma_{33}^2\rangle &= \delta t\\
\langle \delta\Sigma_{11}\rangle = \langle \delta\Sigma_{22}\rangle &= \frac{\delta t}{8}\,[1+3I(\omega)+6I(2\omega)]\\
\langle \delta\Sigma_{33}\rangle &= \frac{\delta t}{4}\,[2+3I(\omega)]\ .
\end{aligned} \tag{4.58}$$

Normalising these by dividing by $\langle \delta\Sigma_{11}^2\rangle$, the anisotropy of the strain field induced by the vorticity is characterised by modified forms for the parameters defined in (4.29) and a scaled value of the parameter $\Delta\mu$ appearing in (4.45):

$$\begin{aligned}
\alpha' &= \frac{1-3I(2\omega)}{1+3I(2\omega)}\\
\beta' &= \frac{3I(2\omega)}{1+3I(2\omega)}\\
\gamma' &= \frac{3I(\omega)}{1+3I(2\omega)}\\
\Delta\mu' &= \frac{3}{2}\frac{1+I(\omega)-2I(2\omega)}{1+3I(2\omega)}\ .
\end{aligned} \tag{4.59}$$

Note that $\alpha' + 2\beta' = 1$, as expected from (4.31). Because $I(0) = 1$, when the vorticity is zero, we have $\alpha' = -1/2$, $\beta' = \gamma' = 3/4$, so that we recover the statistics of an isotropic strain field. In the limit as $\omega \to \infty$ we expect $I(2\omega) \ll I(\omega) \ll 1$, so that to leading order we may set $\alpha = 1$, $\beta = 0$,

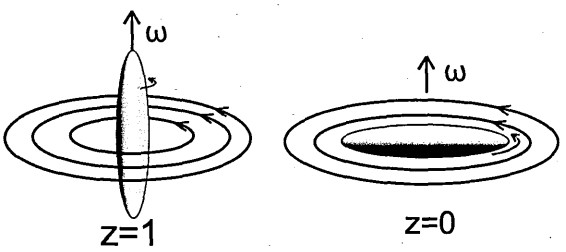

Figure 4.1: Schematic showing principle alignments of the rods with the flow, at the values of $z = 1$ (aligned) and $z = 0$ (anti-aligned), that result from the solution of the analytic model under consideration.

$\Delta\mu = \frac{3}{2}$ and regard γ as a small parameter. Let us consider how to evaluate the probability density function of $z = \mathbf{n} \cdot \mathbf{e}_\omega$ in the limit where $\omega\tau \gg 1$. The general expression for the probability density is equation (4.53). In this limiting case, we may approximate the coefficients α and γ by

$$\alpha \sim 1\,, \quad \gamma \sim \frac{3}{1+\omega^2\tau^2}\,, \quad \Delta\mu \sim \frac{3}{2}\,. \tag{4.60}$$

When $\gamma \ll 1$, the poles $u_\pm$ of the probability density function and the coefficients $c_\pm$ in (4.53) are approximated by

$$\begin{aligned} u_- &\sim -\frac{\gamma}{9} \quad u_+ \sim 1 + \frac{\gamma}{9} \\ c_- &\sim -\frac{1}{2} \quad c_+ \sim -1 \end{aligned} \tag{4.61}$$

so that the probability density function is approximated by

$$P_\omega(z) \sim \mathcal{C}\left(z^2 + \frac{\gamma}{9}\right)^{-1/2}\left(1 + \frac{\gamma}{9} - z^2\right)^{-1} \tag{4.62}$$

where $\mathcal{C}$ is a normalisation constant, and where the subscript ω is a reminder that this distribution is evaluated for a fixed value of ω.

We verified this relation by simulating the orientation of rod-like particles using equations (4.4) and (4.5), using the Ornstein-Uhlenbeck model for the velocity gradients, with the components of the vorticity frozen, so that the only non-zero elements are $\Omega_{12} = -\Omega_{21} \equiv \omega$. The PDF of $z = \mathbf{n} \cdot \mathbf{e}_3$ is plotted in figure 4.2 for $\omega\tau_s = 2$ and $\omega\tau_s = 5$, showing good agreement with the theoretical prediction, equation (4.62).

In figure 4.3 we plot the theoretical PDF of z for three different values of the single dimensionless variable $\omega\tau_s$. For $\omega\tau_s = 1$ we plot both the exact expression obtained from using (4.59) in equations (4.51) -(4.53), as well as the approximate expression (4.62). For the larger values of $\omega\tau_s$ plots of the exact and approximate lie on top of each other. We observe that as $\omega\tau_s \to \infty$ the distribution becomes concentrated around $z = \pm 1$ (rods perfectly aligned with the vorticity) and around $z = 0$ (rods aligned perfectly perpendicular to the vorticity vector). The peak at $z = \pm 1$ is seen to be higher

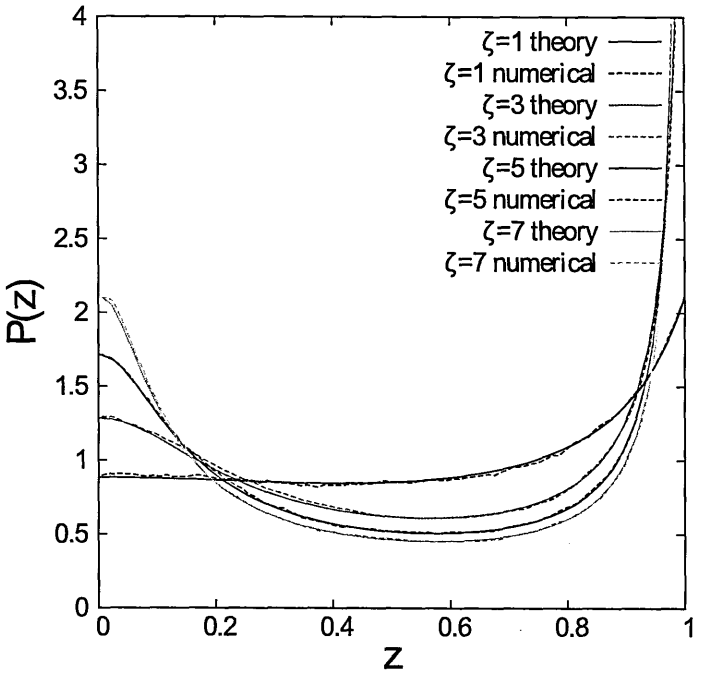

Figure 4.2: Comparison between PDF of $z = \mathbf{n} \cdot \mathbf{e}_3$ obtained by simulation of Jeffery's equation of motion for the random strain model, and the theoretical prediction. In these simulations the vorticity is frozen at $\omega = 1, 3, 5, 7$. The correlation time of the strain fluctuations is $\tau_s = 1$. The numerical simulations used $D_s = 10^{-2}$.

but narrower. In figure 4.4 we plot $\langle |z| \rangle$ and $\langle z^2 \rangle$. Both of these statistics approach $\frac{1}{2}$ in the limit as $\zeta \to \infty$, indicating that in this limit both peaks carry half of the probability.

In practice the magnitude of the vorticity, ω, is not frozen but fluctuates slowly. It has a Gaussian distribution, with a variance $\sigma^2 \equiv \langle \omega^2 \rangle = \frac{3}{4} D_v \tau_v$. Our final estimate for the probability density of z is, therefore, the result on integrating the normalised PDF given by (4.62) over a Gaussian distribution of ω:

$$P(z) = \frac{2}{\sqrt{2\pi}\sigma} \int_0^\infty \mathrm{d}\omega \, \exp(-\omega^2/2\sigma^2) P_\omega(z) \, . \tag{4.63}$$

This PDF depends upon a single dimensionless parameter $\xi = \sigma\tau_s$. The functions obtained by numerical evaluation of the integral in (4.63) are plotted in figure 4.5 for three different values of $\xi = \sigma\tau_s$. We used the exact formulae for $P_\omega(z)$, equations (4.51)-(4.53) and (4.59), because the integral includes the region where $\omega\tau_s$ is small.

4.5 Discussion

We have determined the distribution of $z = \mathbf{n} \cdot \mathbf{e}_\omega$ analytically for a model of microscopic rods in a random velocity field with isotropic statistics. The PDF shows a maximum at $z = 1$ corresponding to alignment parallel to the vorticity, similar to findings of DNS studies of Navier-Stokes turbulence [69].

We conclude by making a few remarks about the relationship between the regime which we have analysed and the velocity gradient statistics for Navier-Stokes turbulence.The model for the velocity

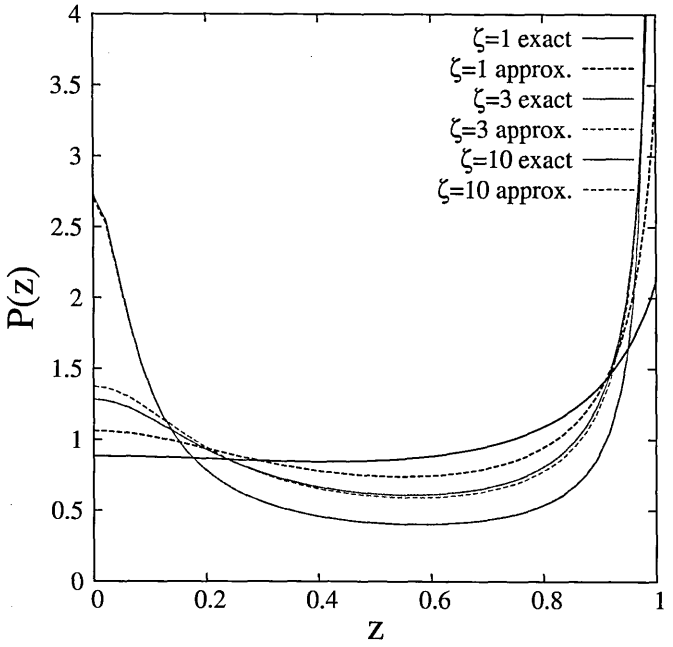

Figure 4.3: Theoretical PDF of $z = \mathbf{n} \cdot \mathbf{e}_3$ for the model where the vorticity is frozen, with magnitude ω. The distribution (4.62) is plotted for three values of $\zeta = \omega\tau_s$, namely $\zeta = 1, 3, 10$. By comparison we have also plotted the exact probability density obtained from equations (4.51)-(4.53) and (4.59). At $\zeta = 10$ the different plots are indistinguishable.

gradient of an isotropic flow which was introduced in section 4.2.2 has four parameters, namely τ_v, τ_s, D_v and D_s, all of which have dimensions which depend only upon time. There are, therefore, three dimensionless parameters. In our analysis the vorticity was frozen, so that $\tau_v \to \infty$. The magnitude of the vorticity, which is of order $\omega \sim \sqrt{D_v\tau_v}$ was chosen so that $\zeta = \omega\tau_s$ is finite. The diffusion coefficient D_s was assumed to be very small, so that the fluctuations of the strain are very small and may be treated using a Fokker-Planck equation.In fact the form of the Navier-Stokes equation restricts the choice of parameters in the Ornstein-Uhlenbeck model for the velocity gradient: it is well known that $\mathrm{tr}(\mathbf{\Omega}^2) + \mathrm{tr}(\mathbf{S}^2) = 0$ [76], which gives a further relation between D_s and D_v. The Navier-Stokes equation also implies that the rate of dissipation per unit mass is $\mathcal{E} = \nu\mathrm{tr}(\mathbf{A}^T\mathbf{A})$, which enables the norm of the velocity gradient to be expressed in terms of the Kolmogorov time, $\tau_K = \sqrt{\nu/\mathcal{E}}$. These results imply the following relations, which determine the ratio of the diffusion coefficients D_s and D_v (see [69]):

$$D_s = \frac{1}{20\tau_K^2\tau_s}\ , \quad D_v = \frac{1}{12\tau_K^2\tau_v}\ . \tag{4.64}$$

Numerical studies indicate that the exponential correlation function is a reasonable model for the statistics of fully developed turbulence, with the parameters τ_s and τ_v satisfying $\tau_s \approx 2.3\tau_K$ and $\tau_v \approx 7.2\tau_K$ (these are the values quoted in [69], which discusses earlier work on the velocity gradient correlation functions). This justifies the assumption that the vorticity is slowly varying, and the variance of the vorticity parameter is estimated to be $\sigma^2 = \langle\omega^2\rangle = \frac{3}{4}\sqrt{D_v\tau_v} = 1/(2\tau_K)$, implying that $\xi = \sigma\tau_s \approx 1.15$ is the value which should be compared with the data on alignment in Navier Stokes turbulence, discussed in [69]. There is a qualitative but not quantitative agreement between the curve

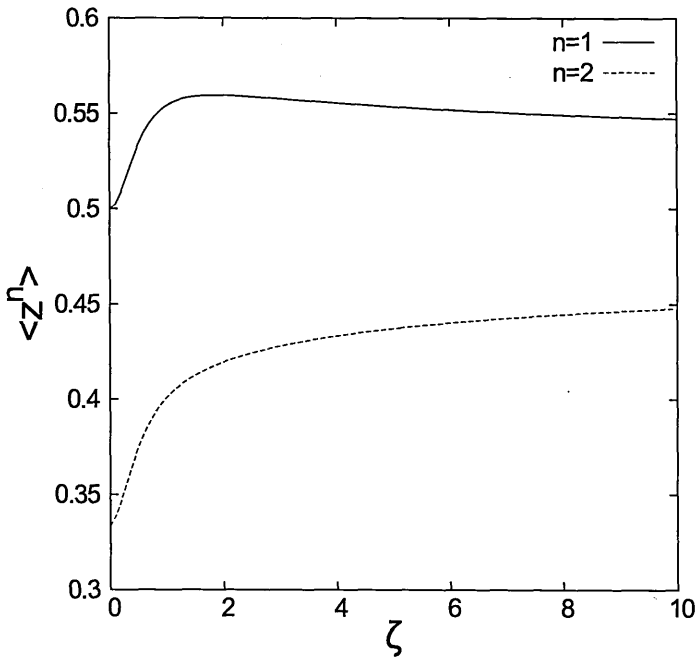

Figure 4.4: Moments $\langle |z| \rangle$ and $\langle z^2 \rangle$ as a function of $\zeta = \omega \tau_s$.

in figure 4.5 for $\xi = 1$ and the results of DNS simulations in figure 2 of [69]: both show a peak in the PDF at $z = 1$, but this peak is more pronounced in the DNS data. We conclude that our model should be understood as a laboratory for understanding alignment of microscopic rods with vorticity, rather than providing a quantitative description.

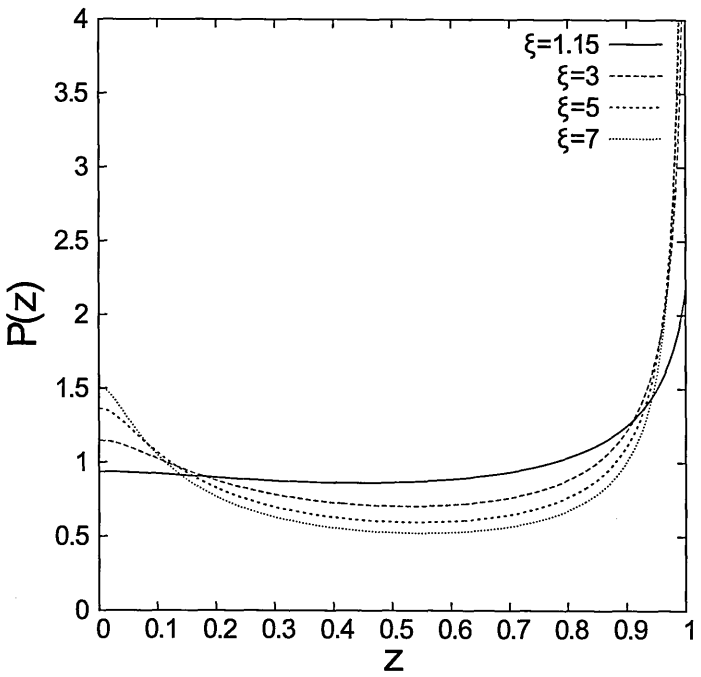

Figure 4.5: Theoretical PDF of $z = \mathbf{n} \cdot \mathbf{e}_3$, averaging over the slowly varying vorticity parameter ω, which is Gaussian distributed with variance $\sigma^2 = \frac{3}{4} D_{\mathrm{v}} \tau_{\mathrm{v}}$. The distribution (4.60) is plotted for four values of $\xi = \sigma \tau_{\mathrm{s}}$, namely $\xi = 1.15, 3, 5, 7$.

Chapter 5

Final remarks

This thesis has addressed two distinct aspects of study concerning particles suspended in quasi-turbulent flows which draw on distinct methodology. The first paper [7] in chapter 3 described a new measure of anisotropy which can be used to distinguish sets which have identical fractal dimensions. Questions regarding the interaction of such sets with electromagnetic radiation remain open, and would constitute a good topic for PhD study. The specific direction of the such study would involve further exploration of two themes.

Firstly, there are questions regarding the interaction simple fractal sets with EM radiation which have been addressed in only a few cases. The paper of Detmann [59] constitutes one such study which involves taking the Fourier Transform of the spatial distribution of points of the cantor set which yields the structure factor, this in turn yields the diffraction intensity. Such an approach was extended in two dimensions by Ferguson [77] and MacKay [78] in which the structure factor of the generalised Sierpinski set is calculated. However, such deterministic fractals are likely to be more manageable than the random fractal which results from inertial particles suspended in turbulent flow. Moreover, the situation is further complicated by the presence of caustics, which is one possible explanation for the divergence between theory and simulation in Wilkinson's paper [35] in which the correlation dimension of the distribution of inertial particles is calculated analytically. The problem of evaluating the spectal dimension of such distribution is likely to much harder, and thus further understanding of not only the structure factor but also the correlation dimension of inertial particles is required before this more intractable problem is addressed. It is likely that it will be some years before general results are found if it is indeed possible that they can be found, especially as the field of fractal physics is at this stage quite mature and it receives little attention in general.

The content of chapter 4, published in [8] constituted a much less open ended topic, since it resulted in a soluble analytic model of ellipsoidal particles in random flow that showed good agreement with simulation but only qualitative agreement with DNS simulations of turbulence. However, in a broader sense, the topic remains a vibrant area of research. Vincenzi's paper [72] gives a discussion of a very

Figure 5.1: Clouds in coffee as a result of the turbulent mixing of colloidal particles contained in the milk with the coffee.

similar model, the work for which was carried out contemporaneously to our own, but considers further generalisations of the shape of particles used and the statistical properties of the flow. Chevillard and Meneveau [79] use Lagrangian particle tracking of generalised ellipsoidal particle in DNS of turbulence and indeed show the motion is distinct from the isotropic field considered in chapter 4. Experimental work being conducted by the group at the Chalmers University of Technology in Gothenburg [80] makes use of the microscopic channel and a shear flow to demonstrate tumbling regimes reminiscent of our work. Extension of this work would consist of progress being made in experimental techniques, as well as DNS of turbulence, in order to give more complete data for particle orientation and behaviour. In summary, we have seen that behaviour of particles in turbulent flows remains a cutting edge field of research in theoretical and experimental Physics alike. Despite making some progress in specific realms, as outlined above, general questions remain open, most famously the existence or otherwise of smooth solutions to the Navier-Stokes equations which remains one of the unsolved Clay Institutes Millennium Prize problems. It is testament to their complexity that the behaviour of natural, at first sight mundane, phenomena such as rain clouds, or even milk as it mixes with coffee 5.1 are not fully understood. Indeed, it is important to remember that, contrary to expectation, extremely challenging Physics remains in everyday phenomena and is not solely contained in the quantum or cosmological regimes.

> I've looked at clouds from both sides now
> From up and down, and still somehow
> It's cloud illusions I recall
> I really don't know clouds at all
>
> *Joni Mitchell* [81]

5.1 Acknowledgements

I would like to thank Professor Michael Wilkinson for his supervision during the bulk of the work and Professor Uwe Grimm for his supervision during the writing-up stage. I would also like to thank the members of the Cambridge-Milton Keynes car share scheme, especially Professor Gillian Rose and Dr Joe Smith, their friendship and guidance was invaluable.

Bibliography

[1] T. S Eliot. The love song of j. alfred prufrock. pages 130–135, 1915.

[2] H.R Pruppacher and J.D Klett. *Microphysics of Clouds and Precipitation.* Springer Berlin Heidelberg, 2010.

[3] P. G. Saffman and J. S. Turner. On the collision of drops in turbulent clouds. *J. Fluid Mech.*, 1(01):16–30, 1956.

[4] Alessandra S. Lanotte, Agnese Seminara, and Federico Toschi. Cloud droplet growth by condensation in homogeneous isotropic turbulence. *J. Atmos. Sci.*, 66(6):1685–1697, 2009.

[5] Florian Janoschek, Federico Toschi, and Jens Harting. Simulations of blood flow in plain cylindrical and constricted vessels with single cell resolution. *Macromolecular Theory and Simulations*, 20(7):562570, 2011.

[6] A. Bracco, P. H. Chavanis, A. Provenzale, and E. A. Spiegel. Particle aggregation in a turbulent keplerian flow. *Phys. Fluids*, 11(8):2280–2287, 1999.

[7] M. Wilkinson, H. R. Kennard, and M. A. Morgan. Spectal dimension of fractal sets. *J. Phys. A: Math. Theor.*, 45(41):415102, 2012.

[8] M. Wilkinson and H. R. Kennard. A model for alignment between microscopic rods and vorticity. *J. Phys. A: Math. Theor.*, 45(45):455502, 2012.

[9] Gregory Falkovich. Cascade and scaling. 3(8):6088, 2008.

[10] Uriel Frisch and A. Andrei Nikolaevich Kolmogorov. *Turbulence: The Legacy of A. N. Kolmogorov.* Cambridge University Press, 1995.

[11] Roger Peyret. *Handbook of computational fluid mechanics.* Academic Press, San Diego, Calif., 2000.

[12] A. Juneja, D. P. Lathrop, K. R. Sreenivasan, and G. Stolovitzky. Synthetic turbulence. *Phys. Rev. E*, 49(6):5179–5194, 1994.

[13] M. R. Maxey. The gravitational settling of aerosol particles in homogeneous turbulence and random flow fields. *Journal of Fluid Mechanics*, 174:441–465, 1987.

[14] J. M. Deutsch. Aggregation-disorder transition induced by fluctuating random forces. *J. Phys. A: Math. Gen.*, 18(9):1449, 1985.

[15] J. Bec, M. Cencini, and R. Hillerbrand. Clustering of heavy particles in the inertial range of turbulence. *arXiv*, (nlin/0606038), 2006.

[16] Piero Olla. Preferential concentration versus clustering in inertial particle transport by random velocity fields. *Physical Review E*, 81(1), 2010.

[17] G Cantor. Über unendliche, lineare punktmannigfaltigkeiten [on infinite, linear point-manifolds (sets)]. *Mathematische Annalen*, 21:545591, 1883.

[18] Benoit B Mandelbrot. *The fractal geometry of nature.* W.H. Freeman, New York, 1983.

[19] K. J Falconer. *Fractal geometry mathematical foundations and applications.* Wiley, Chichester, 2003.

[20] P. Grassberger and I. Procaccia. Measuring the strangeness of strange attractors. *Physica D*, 9:189208, 1983.

[21] G. L Baker and J. B. Gollub. *Chaotic Dynamics: An Introduction, 2nd ed.* Cambridge University Press, 1996.

[22] Athanasios Papoulis. *Probability, random variables, and stochastic processes.* McGraw-Hill, Boston, 2002.

[23] B. Grunbaum. Projection constants. *Transactions of the American Mathematical Society*, 95(3):451, 1960.

[24] R Durrett. *Stochastic Calculus: A Practical Introduction.* CRC Press, 1996.

[25] N. G. van Kampen. *Stochastic processes in physics and chemistry.* North-Holland, Amsterdam; New York, 1992.

[26] Edward Ott. *Chaos in dynamical systems.* Cambridge University Press, Cambridge, U.K.; New York, 2002.

[27] R Rushdi. *Encyclopedia of the history of Arabic science. 1. [Astronomy - theoretical and applied].* Routledge, 1996.

[28] G. I. Taylor. Diffusion by continuous movements. *Proceedings of the London Mathematical Society*, s2-20(1):196–212, 1922.

[29] J.K. Eaton and J.R. Fessler. Preferential concentration of particles by turbulence. *International Journal of Multiphase Flow*, 20, Supplement 1:169–209, 1994.

[30] E. Balkovsky, G. Falkovich, and A. Fouxon. Intermittent distribution of inertial particles in turbulent flows. *Physical Review Letters*, 86:2790–2793, 2001.

[31] J Bec. Fractal clustering of inertial particles in random flows. *Phys. Fluids*, 15(11):L81–L84, 2003.

[32] J Bec. Multifractal concentrations of inertial particles in smooth random flows. *Journal of Fluid Mechanics*, 528:255–277, 2005.

[33] B Mehlig, M Wilkinson, K Duncan, T Weber, and M Ljunggren. Aggregation of inertial particles in random flows. *Phys Rev E Stat Nonlin Soft Matter Phys*, 72(5 Pt 1), 2005.

[34] J. Bec, A. Celani, M. Cencini, and S. Musacchio. Clustering and collisions of heavy particles in random smooth flows. *Phys. Fluids*, 17(7):073301–073301–11, 2005.

[35] M. Wilkinson, B. Mehlig, and K. Gustavsson. Correlation dimension of inertial particles in random flows. *Europhysics Letters*, 89(5):50002, 2010.

[36] J Bec and R Chétrite. Toward a phenomenological approach to the clustering of heavy particles in turbulent flows. *New J. Phys.*, 9(3):77, 2007.

[37] Itzhak Fouxon. The impact of hydrodynamic interactions on the preferential concentration of inertial particles in turbulence. *arXiv*, (1201.2885), 2012.

[38] Kevin Duncan, Bernhard Mehlig, Stellan Ostlund, and Michael Wilkinson. Clustering by mixing flows. *Phys. Rev. Lett.*, 95(24), 2005.

[39] M. Wilkinson, B. Mehlig, S. stlund, and K. P. Duncan. Unmixing in random flows. *Physics of Fluids*, 19(11):113303–113303–23, 2007.

[40] Michael Wilkinson and Alain Pumir. Spherical ornstein-uhlenbeck processes. *J Stat Phys*, 145(1):113–142, 2011.

[41] M. V Berry. Singularities in waves. pages 453–543, 1981.

[42] M. Wilkinson and B. Mehlig. Caustics in turbulent aerosols. *Europhysics Letters*, 71(2):186, 2005.

[43] J. Bec, L. Biferale, M. Cencini, A. S. Lanotte, and F. Toschi. Caustics and intermittency in turbulent suspensions of heavy particles. *arXiv*, 2009.

[44] A. S. Lanotte, J. Bec, L. Biferale, G. Boffetta, A. Celani, M. Cencini, S. Musacchio, and F. Toschi. Acceleration statistics of heavy particles in turbulent flows. In J. M. L. M. Palma and A. Silva Lopes, editors, *Advances in Turbulence XI*, number 117 in Springer Proceedings Physics, pages 115–117. Springer Berlin Heidelberg, 2007.

[45] M. Cencini, J. Bec, L. Biferale, G. Boffetta, A. Celani, A. S. Lanotte, S. Musacchio, and F. Toschi. Dynamics and statistics of heavy particles in turbulent flows. *arXiv*, (nlin/0601027), 2006.

[46] J. Bec, L. Biferale, M. Cencini, A. Lanotte, S. Musacchio, and F. Toschi. Heavy particle concentration in turbulence at dissipative and inertial scales. *Phys. Rev. Lett.*, 98(8):084502, 2007.

[47] J Bec, R Cencini, Mand Hillerbrand, and K Turitsyn. Stochastic suspensions of heavy particles. *Physica D: Nonlinear Phenomena*, 237(1417):2037–2050, 2008.

[48] G. Falkovich, S. Musacchio, L. Piterbarg, and M. Vucelja. Inertial particles driven by a telegraph noise. *arXiv*, (nlin/0703055), 2007. Phys. Rev. E 76, 026313 (2007).

[49] Enrico Calzavarini, Massimo Cencini, Detlef Lohse, and Federico Toschi. Quantifying turbulence-induced segregation of inertial particles. *Phys. Rev. Lett.*, 101(8):084504, 2008.

[50] A Puglisi and M Assaf. Attempted density blowup in a freely cooling dilute granular gas: hydrodynamics versus molecular dynamics. *Physical review. E, Statistical, nonlinear, and soft matter physics*, 77(2 Pt 1):021305, 2008.

[51] Itzhak Fouxon, Baruch Meerson, Michael Assaf, and Eli Livne. Formation of density singularities in ideal hydrodynamics of freely cooling inelastic gases: A family of exact solutions. *Physics of Fluids*, 19(9):093303–093303–17, 2007.

[52] John C. Sommerer and Edward Ott. Particles floating on a moving fluid: A dynamically comprehensible physical fractal. *Science*, 259:335–339, 1993.

[53] T. A. Witten and L. M. Sander. Diffusion-limited aggregation, a kinetic critical phenomenon. *Phys. Rev. Lett.*, 47(19):1400–1403, 1981.

[54] P. Grassberger and I. Procaccia. Dimensions and entropies of strange attractors from a fluctuating dynamics approach. *Physica D: Nonlinear Phenomena*, 13(12):34–54, 1984.

[55] P. Grassberger. Generalizations of the hausdorff dimension of fractal measures. *Physics Letters A*, 107(3):101–105, 1985.

[56] A. Politi, R. Badii, and P. Grassberger. On the geometric structure of non-hyperbolic attractors. *J. Phys. A: Math. Gen.*, 21(15):L763, 1988.

[57] P. Grassberger, R. Badii, and A. Politi. Scaling laws for invariant measures on hyperbolic and nonhyperbolic atractors. *J Stat Phys*, 51(1-2):135–178, 1988.

[58] S.K. Sinha. Scattering from fractal structures. *Physica D: Nonlinear Phenomena*, 38(13):310–314, 1989.

[59] Dettmann, Frankel, and Taucher. Structure factor of cantor sets. *Phys Rev E Stat Phys Plasmas Fluids Relat Interdiscip Topics*, 49(4):3171–3178, 1994. PMID: 9961585.

[60] Thomas C. Halsey, Mogens H. Jensen, Leo P. Kadanoff, Itamar Procaccia, and Boris I. Shraiman. Fractal measures and their singularities: The characterization of strange sets. *Phys. Rev. A*, 33(2):1141–1151, 1986.

[61] T Bedford. Crinkly curves, markov partitions and dimension. 1984.

[62] C McMullen. *Nagoya Math. J*, 96:1–9, 1984.

[63] G. B. Jeffery. The motion of ellipsoidal particles immersed in a viscous fluid. *Proc. R. Soc. Lond. A*, 102(715):161–179, 1922.

[64] F. P. Bretherton. The motion of rigid particles in a shear flow at low reynolds number. *Journal of Fluid Mechanics*, 14(02):284–304, 1962.

[65] E. J. Hinch and L. G. Leal. The effect of brownian motion on the rheological properties of a suspension of non-spherical particles. *Journal of Fluid Mechanics*, 52(04):683–712, 1972.

[66] Michael Wilkinson, Vlad Bezuglyy, and Bernhard Mehlig. Fingerprints of random flows? 21(4):043304–043304–11, 2009.

[67] Shima Parsa, Jeffrey S. Guasto, Monica Kishore, Nicholas T. Ouellette, J. P. Gollub, and Greg A. Voth. Rotation and alignment of rods in two-dimensional chaotic flow. *Physics of Fluids*, 23(4):043302–043302–10, 2011.

[68] Y. N. Mishra, J. Einarsson, O. A. John, P. Andersson, B. Mehlig, and D. Hanstorp. A microfluidic device for studies of the orientational dynamics of microrods. pages 825109–825109, 2012.

[69] Alain Pumir and Michael Wilkinson. Orientation statistics of small particles in turbulence. *New J. Phys.*, 13(9):093030, 2011.

[70] S. S. Girimaji and S. B. Pope. A diffusion model for velocity gradients in turbulence. *Physics of Fluids*, 2(2):242–256, 1990.

[71] Brett K. Brunk, Donald L. Koch, and Leonard W. Lion. Turbulent coagulation of colloidal particles. *Journal of Fluid Mechanics*, 364:81–113, 1998.

[72] Dario Vincenzi. Orientation of non-spherical particles in an axisymmetric random flow. *Journal of Fluid Mechanics*, 719:465–487, 2013.

[73] Andrew J. Szeri. Pattern formation in recirculating flows of suspensions of orientable particles. *Phil. Trans. R. Soc. Lond. A*, 345(1677):477–506, 1993.

[74] Dario Vincenzi, Shi Jin, Eberhard Bodenschatz, and Lance R. Collins. Stretching of polymers in isotropic turbulence: A statistical closure. *Phys. Rev. Lett.*, 98(2):024503, 2007.

[75] G. E. Uhlenbeck and L. S. Ornstein. On the theory of the brownian motion. *Phys. Rev.*, 36(5):823–841, 1930.

[76] R. Betchov. An inequality concerning the production of vorticity in isotropic turbulence. *Journal of Fluid Mechanics*, 1(05):497–504, 1956.

[77] A Ferguson, T Jordan, and P Shmerkin. The hausdorff dimension of the projections of self-affine carpets. *Fund. Math*, 209.

[78] J M Mackay. Assouad dimension of self-affine carpets. *Conform. Geom. Dyn.*, 15.

[79] Laurent Chevillard and Charles Meneveau. Orientation dynamics of small, triaxial-ellipsoidal particles in isotropic turbulence. *arXiv*, (1305.6275), 2013.

[80] J. Einarsson, A. Johansson, S. K. Mahato, Y. Mishra, J. R. Angilella, D. Hanstorp, and B. Mehlig. Aperiodic tumbling of microrods advected in a microchannel flow. *arXiv*, (1211.5672), 2012.

[81] Joni Mitchell. Both sides now. *Reprise Records*, Clouds, 1969.